UiA University of Agder

Master

Evaluating The Performance Of Wind Farm Wake Models Using The Performance Data From A Land-Based Wind Farm

Karen María Jensdóttir

Supervisors
Sathyajith Mathew
Ghali Raja Yakoub

University of Agder, 2020
Faculty of Engineering and Science
Department of Engineering Sciences

Abstract

Performance data from the Wind R&D Park on Prince Edward Island in Canada has been used to validate three different far-wake kinematic wake models. The wake models that have been compared are the Jensen, Larsen, and Ishihara wake models. The study was conducted for a total of 27 cases. The cases were for the velocity bands 3-7 m/s, 7-11 m/s, and 11-15 m/s. For each of these velocity bands the directional band $230 - 320°$. Within that directional band, simulations were performed with $10°$ intervals. This directional band was chosen due to it being the dominant wind direction of the wind farm, the simulations were done using WindSim. The Larsen model correlated best with the measured values. The Ishihara and Jensen wake models gave similar results. The Ishihara model correlated better with the measured data than the Jensen model. From the error calculations, it was seen that as the velocity increased the more accurate the simulated values became. The directional bands of $230° - 240°$ and $240 - 250°$ for the velocity band 3-7 m/s, and the directional band $230 - 240°$ for the velocity band 7-11 m/s, showed the largest error between the measured and simulated values. This error was not displayed for these directional bands for the velocity band 11-15 m/s as the simulations showed more accuracy for that velocity band, as the rated velocity is in that velocity band. WindSim is an adequate wind farm design tool (WFDT) for wake loss simulations and gave acceptable results for a wind farm the size of the Wind R&D Park.

Preface

First of all I would like to thank Wind Energy Institute of Canada (WEICan) and Carrie Houston for allowing me to use the data from the Wind R&D Park. Without this contribution this thesis would have been impossible to accomplish.

I would like to thank my supervisors. Sathyajith Mathew thank you for offering me such a motivating thesis topic and your guidance through my writing. I would also like to thank you for inspiring me through your lectures for my passion for wind energy. To Ghali Raja Yakoub thank your for your patience and the help you gave me in learning on the software needed to complete the thesis.

I would also like to express my thanks to Muhammad Bilal for your help and input.

During my two year study at the University of Agder, the support of my friends has been very important. Thank you for all the support and the laughs that have carried me through these past two years.

Last but not least, I would like to thank my parents Guðrún Ýrr Tómasóttir and Jens Kristján Kristinsson, my boyfriend Brynjar Bragason, and Dangný Björk Reynisdóttir thank you for your support, wisdom, and kindness.

Individual/group Mandatory Declaration

The individual student or group of students is responsible for the use of legal tools, guidelines for using these and rules on source usage. The statement will make the students aware of their responsibilities and the consequences of cheating. Missing statement does not release students from their responsibility.

1.	I/We hereby declare that my/our report is my/our own work and that I/We have not used any other sources or have received any other help than mentioned in the report.	☒
2.	I/we further declare that this report: - has not been used for another exam at another department/university/ university college in Norway or abroad; - does not refer to the work of others without it being stated; - does not refer to own previous work without it being stated; - have all the references given in the literature list; - is not a copy, duplicate or copy of another's work or manuscript.	☒
3.	I/we am/are aware that violation of the above is regarded as cheating and may result in cancellation of exams and exclusion from universities and colleges in Norway, see Universitets- og høgskoleloven §§ 4-7 og 4-8 og Forskrift om eksamen §§ 31.	☒
4.	I/we am/are aware that all submitted reports may be checked for plagiarism.	☒
5.	I/we am/are aware that the University of Agder will deal with all cases where there is suspicion of cheating according to the university's guidelines for dealing with cases of cheating.	☒
6.	I/we have incorporated the rules and guidelines in the use of sources and references on the library's web pages.	☒

Publishing Agreement

Authorization for electronic publishing of the report.

Author(s) have copyrights of the report. This means, among other things, the exclusive right to make the work available to the general public (Åndsverkloven. § 2).

All theses that fulfill the criteria will be registered and published in Brage Aura and on UiA's web pages with author's approval.

Reports that are not public or are confidential will not be published.

I hereby give the University of Agder a free right to
make the task available for electronic publishing: ☐ JA ☒ NEI

Is the report confidential? ☒ JA ☐ NEI
(confidential agreement must be completed and signed by the Head of the Department)

- If yes:

Can the report be published when the confidentiality period is over? ☒ JA ☐ NEI

Is the task except for public disclosure? ☐ JA ☒ NEI
(contains confidential information. see Offl. § 13/Fvl. § 13)

Contents

List of Figures

List of Tables

Notation

Latin Symbols

$\overline{a}$	Average induction factor
d_{ij}	Distance between the centers of a downstream wind turbine
f_i	External body force
h	Wind turbine hub height
i	Directional component i
j	Directional component j
k	Wake decay factor
obs	Observed value
$\overline{obs}$	Average observed value
r	Wake radius
r_0	Rotor radius
r_i	Radius of the wake behind a upstream wind turbine
sim	Simulated value
t	Time
u	Velocity
v	Kinematic viscosity
v_0	Free-stream velocity
v_i	Resulting velocity from a wind turbine in multiple wake situation
v_t	Turbulent kinematic viscosity
v_w	Wake velocity
x	Position vector
x_d	Downstream distance
x_{ij}	Distance between a upstream and downstream wind turbines
z	Coordinate in the vertical direction

z_0	Surface roughness
A_0	Area of the wind turbine experiencing shadowing
A_i	Surface area of the cell facing the undisturbed wind flow direction
$A_{shadow,i}$	Area spanned by the wake shadow
C_T	Thrust coefficient
D	Rotor diameter
F_i	Force thrust
I_a	Ambient turbulence intensity
K	Turbulent kinetic energy
M	Number of upstream rotors
P	Pressure
P_E	Power production
P_{E1}	Power production of wind turbine 1
P_{Ei}	Power production of wind turbine i
P_{max}	Maximum power production
P_N	Normalized power production
R_w	Radius of the expanding wake
S_{ij}	Strain rate tensor
T_0	Shear stress
U	Incoming ambient velocity
$\overline{U}$	Velocity of a wind farm (non-linear)
$U_{1,i}$	Velocity of the flow at i-th cell
$\overline{U}_m$	Velocity of a wind farm (linear)
U_T	Friction velocity
U_∞	Inflow velocity

Greek Symbols

α	Decay constant
α_i	Axial induction factor
δV	Normalized velocity deficit
ε	Dissipation rate
κ	The von Karman constant
ρ	Fluid density

Abbreviations

ADM	Actuator-Disc Model
ADM-R	Actuator-Disc Model With Rotation
AEP	Average Energy Production
BEM	Blade Element Momentum
CFD	Computational Fluid Dynamics
DTU	Technical University of Denmark
GIS	Geographic Information System
HAWT	Horizontal Axis Wind Turbine
KE	Kinetic Energy
LES	Large-Eddy Simulations
MAE	Mean Absolute Error
NDA	Non-Disclosure Agreement
NRMSE	Normalized Root Mean Square Error
RANS	The Reynolds-Average Navier-Stokes equation
RMSE	Root Mean Square Error
RNG	Re-Normalization Group
VAWT	Vertical Axis Wind Turbine
WAsP	Wind Atlas Analysis and Application Program
WEICan	Wind Energy Institute of Canada
WFDT	Wind Farm Design Tool
WFOG	Wind Farm Optimization Using a Genetic Algorithm

1 Introduction

1.1 Background and Motivation

Wind turbines are often installed in clusters with minimal distance between each other. This is called a wind farm. Which is executed due to limitations of good sites and to lower the cost of transmission lines and maintenance. Grouping the wind turbines has shown to be problematic. One of those problems is the wake loss that occurs after the wind flows through the blades of the wind turbine.[1] Since the wind turbines extract the energy from the wind to generate electricity, it makes sense that the wind on the other side of the wind turbine has lower energy [2]. Due to this the wind downstream of the wind turbine is turbulent and has lower wind speed, this is what is called the wake effect of a wind turbine.[3]

It is important to consider the wake effect when designing a wind farm as it can have a lot to say to maximize the energy output and lifetime of the wind turbines. Many numerical models of varying complexity have been developed to describe the wake effect. All these models can be classified as either explicit or implicit [4]. The explicit also known as kinematic wake models use self-similar velocity profiles determined semi-empirically [5, 6, 7]. The implicit wake models were developed as an elaborate alternative to the explicit wake models. The implicit wake models are all based on approximations of either the Navier-Stokes or vorticity transport equations [3]. For the modeling of wind farms, wind speed distribution is a complex task and many of the parameters that are needed to gain an accurate result are not readily available [2]. The choice of a suitable wake model depends on three factors. (1) the desired computational time, (2) the necessary accuracy of prediction, and (3) the available wind modeling parameters. [3]

There are a few key elements that need to be taken into account when it comes to wake loss from wind turbines. Figure 1.1 shows the parameters that affect the wake and need to be taken into consideration when minimizing the wake effect. As can be seen from the figure, many aspects of designing a wind farm affect the wake losses and thus the efficiency of the wind farm. These are just the main parameters that affect the wake and not all of them. The distance between the turbines needs to be right, not too long and not too short. If the space is too short then the turbine is located in the region where the wake losses are high and could also be affected by turbulence, and therefore produce less power than anticipated. If the spacing is too long then there may be space for fewer turbines in the wind farm than there could be, and thus making the total power production of the wind farm lower. The wind speed and direction of the wind farm are important. Facing the wind turbine in the dominant direction of the wind is an

important factor in minimizing the wake, as the wake can be of different magnitude, depending on where the wind hits the turbine blades. The wind speed is important for the same reason. The placement of the turbine in the wind farm needs to be according to the dominant wind speed of the location. Different wind velocity can generate wake loss of different magnitudes. The land surface is important to take into account, especially if it has hills or trees for example. These elements can make the wind turbulent. If the wind hits the turbine with turbulence, less power will be generated. The roughness of the land surface also indicates at which height the turbine will be in when it comes to the boundary layer.

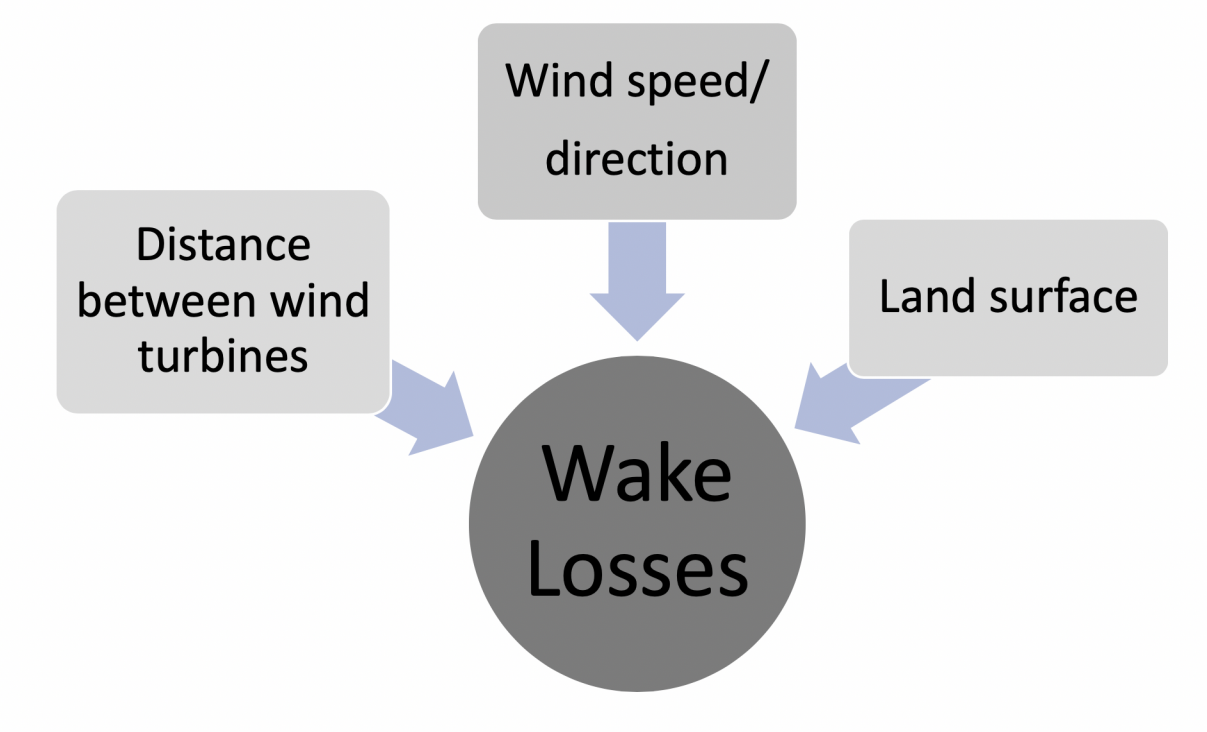

Figure 1.1: Flow chart showing the factors that affect wake losses

In this project simulations of wake effect have been completed, where the wake will be simulated with three different wake models that are available in WindSim. The wind farm that was analyzed is the Wind R&D Park located on Prince Edward Island in Canada, which is a 10MW wind farm that contains five 2MW wind turbines. The Wind R&D Park is owned by the Wind Energy Institute of Canada also known as WEICan. WEICan is a not-for-profit institute and governed by a volunteer board of directors. The institute is self-sufficient through the sales of the power from the Wind R&D Park [8]. The Jensen, Larsen, and Ishihara wake models will be compared in this study. The aim is to find which one of the wake models gives the most accurate results when compared to the measured data from the wind farm. To do this the wake loss in the wind farm will be analyzed at specific velocity bands, which are 3-7 m/s, 7-11 m/s, and 11-15 m/s. In these velocity bands simulations were made for every 10° from 230° to 320°.

1.2 Steps Involved

There are three steps involved to execute this project. The first step is to clean the data obtained from the Wind R&D Park in Canada, both for the simulations and the power production of each wind turbine. Then the data is divided into the velocity and directional bands. This needs to be completed to make the climatology files needed for the project. The second step is to run the simulations for all the velocity and directional bands. The third and final step is to work with the results from the simulations and compare them with the measured data from the wind turbines, along with error calculations.

1.3 Research Question and Problem Statement

In this report, the following research questions will be analyzed and answered.

1. How can the wake effect in a wind farm be modeled using WindSim?
2. How do these wake estimates compare with the actual observations?
3. How does WindSim perform in different velocity bands corresponding to the performance regions of a turbine?

1.4 Report Structure

The report is structured as follows: In chapter 2 research of literature, in the field of wake effect in wind energy is reviewed to detect what others have accomplished in the same field. Chapter 3 explains the theories which are relevant to the project. Chapter 4 describes the method used in this project. Chapter 5 displays the results obtained during the project. In chapter 6 the results will be discussed and thoughts on any issues will be inclined. In chapter 7 the conclusion of the results from the project will be given. Chapter 8 inspects what opportunities there are for further research.

2 | Review of Literature

Planning and building a wind farm takes many important steps, forethought, time, and funding. Therefore it is important to research and analyze new revelations in wind energy. Wind energy has been fast growing over the past decade and, as a result the field has evolved considerably. In this project, the focus will be on wind turbine wake effect and its behavior in wind farms. Since this will be the main focus of this project, this chapter will also focus on researches where the focal point is the wake effect and the use of different wake models. Furthermore, a focus will be on research with wake effect using WindSim, since that will be the program used in this project.

2.1 Wake Studies In Wind Farms

Wake effect plays a big role in wind farm design, including finding the optimum capacity of a wind farm with regards to the location. Because of this, it is important to look into what is happening in wake effect evolution and how other researchers are measuring and calculating the wake losses in wind farms, and how they are maximizing the area of the farm.

In a study conducted by Mo *et. al* 2013, a Large Eddy Simulation (LES) was performed on a wind turbine which was placed two rotor diameters from the upstream boundary with a downstream domain of 20 rotor diameters, the tests were completed at different velocities 7 m/s, 10 m/s, 13.1 m/s, and 15.1 m/s. This was done using the CFD software ANSYS FLUENT. The results from the simulations were compared to experimental data published by the NREL. The researchers observed that the wake behind the turbine consisted of an intense and stable rotating helical vortices. From the simulation, it was concluded that the downstream distance that the wake instability and vortex breakdown happens was the function of the upstream wind speed. Furthermore, the researchers observed that the turbulence intensity rapidly decreased during the wake instability and vortex breakdown. It was concluded that the location of the decrease is a function of the upstream wind speed. The researchers also suggested that the distinction between the near- and far-wake regions could be identified as the average location between the start of the wake instability and the end of the process of the breakdown. The comparison of the simulated and experimental data seemed to be in good agreement. [9]

De-Prada-Gil *et. al* 2015, did a study where the potential benefit of a wind farm control strategy whose main object was to maximize the total energy yield over its lifetime by considering that

the wake effect in the wind farm varies depending on the operation of each wind turbine. The researchers proposed that the control strategy optimize the whole system by operating some wind turbines at sub-optimum points. This was done to reduce the wake effect within the wind farm, and with that maximize the total power generation. This was conducted for two different wind roses. one wind rose was only at 90° and the other wind rose had data for every 30°. The study takes into account the blade element momentum (BEM) theory. It also includes a comprehensive wake model considering single, partial, and multiple wake effects. The researchers concluded that by using the control strategy the annual energy capacity of the wind farm could go from $1,86\%$ to $6,24\%$ (depending on the wind farm) with operating specific wind turbines slightly away from their optimum point and therefore reducing the wake effect. [10]

Zuo *et. al* 2016, conducted a study where an unsteady numerical simulation was performed to investigate the wake structure of a three-bladed H-type vertical axis wind turbine (VAWT). The researchers performed the study with a simplified two-dimensional model, which considered that the blades of the turbine are straight. An unsteady Reynolds Average Navier-Stokes (RANS) equation was solved using the software FlowVision. The researchers concluded that the velocity recovery distance needed for a VAWT is normally larger than 15D, it is important to note that this is much larger than for a horizontal axis wind turbine (HAWT). In this study the distance between the wind turbines was from 5D to 17D with 2D intervals. Where D is the rotor diameter. [11]

In a study done by Li *et. al* 2018, field measurements and a wake model was based on experimental data to analyse the wake characteristics of a horizontal axis turbine in a wind farm. The researchers examined the wake flow at different tip speed ratios and pitch angles. The pitch angles used were $\beta = 0°, 2°$ and $4°$. The wind velocity ratios were $U_{NR} = 0,83, 0,78$ and $0,75$ The wake velocity distribution was also predicted using a wake model with Gaussian function. The researchers concluded that the study provided a better understanding of wake characteristics in the field. For the location of the study the wind direction difference between the inflow in the mainstream direction and the wake flow becomes larger towards the hill direction of the area. The researchers stated through that the limitations of the results are that the prediction made are only at the location of the wind turbine. [12]

2.2 Wake Models

When simulating and researching the wake effect of a site, so-called wake models are often used. There are different types of wake models. Variant types of wake models are used under different circumstances, depending on their aim. In this chapter studies using variant wake models will be reviewed.

González-Longatt *et. al* 2011, conducted a study where a simplified explicit model of wake effects was presented by using the Jensen wake model for multiple wakes. These models included the cumulative impact of multiple shadowing, the effects of wind direction and wind speed time delays. These models were done using Matlab. The model was then integrated into a power system simulation for a wind farm to analyze the effect of wake on the wind farm, particularly in terms of the wake coefficient and overall active power losses. The researchers decided to analyze the steady-state long term effect in the model, as well as the dynamic short-term effect of the wake effect on the wind farms. The results showed that the spacing between the turbines was important when it came to the wake effect and the wind farms' power production. When the researchers increased the spacing between the turbines the performance of the steady-state and dynamic simulations improved for the power output of the wind farm. Furthermore, the dynamic simulations that were performed demonstrated that with bigger spacing between the turbines the resulting increase in electrical losses was minimal compared to the increase in the power drawn from the wind. [3]

Mittal *et. al* 2011, conducted a study where two wake models were compared. The models that were compared were the Jensen wake model and the Ishihara wake model. To conduct the study, data from two offshore wind farms Horns Rev and Nysted were used. The study was conducted using wind farm optimization using a genetic algorithm (WFOG), which is a code developed in Matlab. The researchers concluded that the Ishihara wake model estimated the velocity in the wake more accurately than the Jensen wake model did. This could stem from the fact that the Ishihara model uses more physics. It takes into account the effect of atmospheric turbulence and the rotor generated turbulence leading to a variable rate of recovery compared to a constant recovery in the Jensen model. [13]

Charhouni *et. al* 2015, conducted a study on three wake models Jensen, Ishihara, and Frandsen. The research aimed to predict the wind velocity in the wake region of the wind turbines. The researchers stated that the Jensen wake model is the most parsimonious due to its few equations and parameters. Making the Jensen wake model the simplest of the three models. The Frandsen wake model was found to be least parsimonious, making it the most complex out of the three models due to the large number of equations and parameters. The researchers measured the accuracy of the wake models to find which one was the most reliable. To do this the off-shore wind farm Horns Rev in Denmark was used. It was found that in the Jensen and Frandsen wake models it is the wake decay constant and thrust coefficient that causes under- or over-prediction and thereby causing inaccuracy. On the other hand, the Ishihara wake model takes into account the effect of turbulence without including the roughness, this may be the cause for inaccuracy in the model. The researchers concluded that none of the wake models that were studied could

estimate the wind velocity deficit accurately. Out of the three, the Jensen wake model, according to the study was the model that gave a good argument in terms of the criteria studied. As stated in the report further research into the wake model uncertainty is required and the next step is to use the fuzzy approach. [14]

Shakoor *et. al* 2016, conducted a study where different types of far-wake models were compared to each other. The models that the researchers compared were Jensen's model, Larsen's model, Frandsen's model, 2D field models, and three-dimensional field models. The researchers found that for all the wake models the spacing and downstream distance between the wind turbines had the most effect on the wake loss. It was concluded that the Jensen wake model gave the most accurate results. This model gave an acceptable degree of prediction accuracy for the off-shore and land-based flat terrain wind farms. Furthermore, the researchers found that it is particularly difficult to predict the accuracy of specific models or groups of models for multiple wakes. The capability for wake models to predict atmospheric and sea stability effects and losses due to nearby wind farms appear to be lacking. [15]

In a study done by Göçmen *et. al* 2016, wake models were described and their sub-components analyzed. The wake models were Jensen, Larsen, Dynamic wake meandering, Fuga, Ellipsys3D, and RANS model. All of these models were developed at the Technical University of Denmark (DTU). In this study the models were evaluated using data from two wind farms, Sexbierum which is an on-shore wind farm, and Lillgrund which is an off-shore wind farm. This was done to compare the model's performance for both cases. To analyze the different wake models at the two locations, the researchers applied benchmarks. In the case of Sexbierum two benchmarks were defined. Single and double wake cases. For Lillgrund four benchmark cases were made, sector variation, speed recovery, power deficit as a function of turbulence intensity, and park efficiency. The researchers concluded that the Jensen, Larsen, and Fuga models were convenient for large wind farm calculations, due to their robust and computational affordability. The Ellipsys3D and RANS models gave good results. But due to their computational cost they are very rarely implemented on large wind farms and their application was found to be limited to the near wake region or to highly complex flows. From the benchmark studies the researchers concluded that the introduction of the wind direction uncertainty improves the accuracy of the power predictions of the Jensen, Larsen, and Fuga models for the Lillgrund case. For Sexbierum the Ellipsys3D model faild to reproduce the depth of the wake deficit. [16]

In a study conducted by Sun *et. al* 2018, three wake models were compared. The models chosen were the Jensen wake model, two-dimensional (2D) Jensen wake model, and the Jensen-Gaussian wake model. The study was performed on a 200 MW offshore wind farm in the Waglan Island sea area in Hong Kong. The researchers concluded that the Jensen wake model overestimated the power losses. The 2D Jensen wake models total power estimation was higher than of the Jensen wake model. For the Jensen-Gaussian wake model, the power estimation depended on the wind turbine's position, but for most of them, the power estimation was less than of the Jensen wake model. The researchers stated that the impact from the wake on the wind turbines structure deserves more attention than mainly looking at the power estimation. This was found to be important since the structural integrity of the wind turbines can affect the wind farm's

economical efficiency. Further research discussed in the report, was to study the 3D Jensen-Gaussian wake model, which is a new wake model and will integrate the 2D Jensen wake model, and the Jensen-Gaussian wake model and is expected to describe wake characteristics more precisely. It was also discussed that the wake's impact on the wind turbine structure would be studied further. [17]

In a study done by Sadaghatizadeh *et. al* 2018, numerical models were used to develop wind turbine wakes using large-Eddy simulation (LES), Jensen, Frandsen, 1st Larsen, and 2nd Larsen models. Where the models were tested against experimental data. THe CFD program ICEM was used in the study to create a hexahedral mesh on the turbine blades in the cylindrical zone. The researchers concluded that the models over-predicted the wake expansion and under-estimated the velocity recovery rate. This, in turn could result in a wind farm with fewer wind turbines and thus generate less power. The researchers stated that the LES model can be used to get information about the flow field, which can be used to plan a wind farm that operates under optimum conditions in terms of power production and maintenance cost. [1]

2.3 Wake Modeling Using WindSim

Since this project is being executed in the program WindSim, it is important to research what other researchers have been studying by using the same program where the wake effect from the wind turbines is the main focus. WindSim can be used for many other applications in wind farm projects other than just studying the wake effect. Other usability is noise calculations, annual power production, and wind farm design.

Crasto *et. al* 2012, did a study where the wakes induced by the wind turbines were modeled. The researchers split the study in two parts. In the first part, series of simulations were conducted over a single wind turbine to perform a grid sensitivity study. In the second part, a validation against the production data was presented from the off-shore wind farm Horns Rev. The actuator disc concept was applied to the wind turbines in combination with RANS simulations. Three ways of dierent pressure drops over the disc of the turbines, were applied. They were uniform, parabolic, and polynomial. The pressure drop was calculated from the thrust coefficient and the axial induction factor from the Betz's theory. Also, two methods were used to compute the power. The first one was to extract the wind speed at the rotor and applying the power curve. The second one was to compute the integral of the power extracted by the disc. The researchers compared the simulation results with the Horns Rev production data at 6 and 10 m/s. It was concluded that the power drop within the first and second rows were predicted within acceptable approximations. It was also found that the actuator disc model gave better results for power predictions at higher wind speeds and wider directional sectors. It is mentioned, that since the actuator disc model doesn't give as accurate conclusions from narrower sectors, it could be possible that the meandering should be included by unsteady RANS. It is mentioned that the swirl of the wake can play an important role on the wake simulation and will need further research. [18]

In a study conducted by Castellani *et. al* 2013, a CFD model was made of the wind farm

Sexbierum in the northern part of the Netherlands. By using the actuator disc wake model to understand the wind behaviour in a complex wind farm. The study was split into two sections. The simulated data where seven meteorological masts were installed to measure the undisturbed wind conditions from each direction. The second section was the experimental data. The researchers concluded that for the single wake the simulated and experimental data seemed to be in good agreement. However the simplifications to the actuator disc wake model in WindSim didn't allow for reliable results for the near-wake zone of the wind turbines. The researchers stated that this could be due to the speed decits, reproduced by the actuator disc wake model. They may be too focused in the wake core, which can be because of the lack of turbulent momentum exchange. The study showed, however, that despite the simplications in the physical model, doing these types of models can give a useful contribution for understanding the complex aerodynamics of large o-shore wind farms. Furthermore, the power output of each rotor, wind speed and the turbulent kinetic energy are key parameters to be supervised when modeling a wind farm. [19]

Castellani *et. al* 2013, conducted a study where the actuator disc model was implemented to simulate the wakes of a wind farm. For the study, real performance data was used from a small wind farm located in the western coastal region of Finland. The researchers found that using a simulation program such as WindSim can be useful to simulate the wind turbines wakes and their interaction with the main wind field. The researchers also disclaimed that the model used in this study had higher accuracy than the one of traditional analytical wake models. The model though, was not proposed for extensive wake simulations, but an estimation of the power losses of a wind farm. A few improvements were recommended for the model, such as introducing different types of thrust force distribution, developing the simulation of turbulence by using different models and lastly, to introduce rotational effects. [20]

Simisiroglou *et. al* 2014, did a study on how different grid resolutions, inflow angles, thrust radial distribution, and turbulence closure models can affect the individual energy production of the wind turbines. This study was done with data from the off-shore wind farm Lillgrund. In this study the actuator disk method was used. The results displayed in the report were for rows 3 and 5 of the wind farm with an inflow angle of 120°. For rows B, D, and E the inflow angle was at 222°. It was concluded that there was an overestimation of wake loss especially when using the Re-normalization group (RNG) k-epsilon turbulence model. The researchers stated that the overestimation of the model could be due to the assumption of the neutrally stratified atmospheric boundary layer in the simulation that is not the general case in reality. Also when using standard k-epsilon, modied k-epsilon and k-epsilon with YAP correction, using the polynomial distribution of the thrust, it seemed that the models tended to overestimate the power output of the rst and second wind turbines in the row. On the other hand a more accurate power output of the subsequent wind turbines was more accurate than when using the RNG k-epsilon model. To continue this research the researchers discuss conducting further research on the first three wind turbines in the row. It could also be good practice to look at more than just rows 3 and 5 and look at more of the turbines of the wind park. [21]

In a study performed by Wu *et. al* 2014, a modeling framework was proposed on wind turbine

wakes and power losses due to the wakes at Horns Rev. In the study LES with blade element theory and a turbine-model-specific relationship between shaft torque and rotational speed was used. The results were then compared with the results from two simulation software WindSim and wind atlas analysis and application program (WAsP). The power output and forces of the wind turbines were modeled using two different approaches. The first approach was the traditional actuator-disc without rotation (ADM-NR). The second approach was an actuator-disc model with rotation (ADM-R). The researchers found that a more accurate result is shown using dynamic ADM-R than with the standard ADM. The wind farm simulation software WindSim and WAsP were also found to underestimate the power output compared with the results from the proposed LES framework. [22]

In a study conducted by Seim *et. al* 2017, three different kinematic wake models were validated using real data from the wind farm Nygårdsfjellet in Norway. The three wake models which were validated, were the Jensen-, Larsen- and Ishihara wake models. The validation was performed in the CFD program WindSim. The researchers concluded that for the location of the study the Larsen wake model gave the most accurate results. The Larsen model though, tended to overestimate the width of the wake and underestimate the energy loss. The Jensen model proved to be reasonably accurate while the Ishihara model showed clear signs of overestimating the energy losses. It is mentioned that it is not possible to estimate which model is the most accurate, due to terrain issues and uncertainty in the measurements. [23]

2.4 Conclusion for Literature Review

From the studies reviewed in this chapter, it was evident that many researchers test more than one wake model in their studies, as different wake models can give variating results depending on the layout and terrain of the wind farm. This means that one wake model is not necessarily better than the other. Furthermore, on-land and offshore wind farms are often studied together to analyze the difference in wake losses and the performance of the wake models.

WindSim is widely used for wake effect simulations and gives reasonable results that can give a good idea to the wake behavior and power losses due to wake effect. It is though stated in many of the studies that the three wake models in WindSim seem to be under- or overestimating the power losses. To sum it up WindSim is an efficient simulation program to give a general picture of the wake effects and power losses, but if more detailed conclusions are needed, more detailed oriented programs should be used.

Many studies look into the wake effect for the whole wind farm, or look into the wake of chosen turbines and study their wake behavior. Not many studies analyze the wake from different directional bands or see the wakes' behavior at specific velocities. In this study this will be looked closer into, to see how the wake changes at different directions and velocities.

3 | Theory

3.1 Wake Effect

The wake effect from a wind turbine is categorized into two regions, which are the near-wake and the far-wake. The near-wake starts right behind the wind turbine and extends to approximately 2-4 rotor diameters. In the near-wake region, the flow of the wind is highly influenced by the rotor geometry, which leads to the formation of the blade tip vortices. There are also formed steep gradients of pressure and axial velocity, and wake expansion in the near wake region. [16]

In the far-wake region, the effects of the rotor geometry are limited, to the reduced wind speeds and increased turbulence intensity. For the far-wake region, the turbulence is the dominating property [24]. The near-wake and far-wake are illustrated in 3.1. Where the regions of the near- and far-wake are displayed.

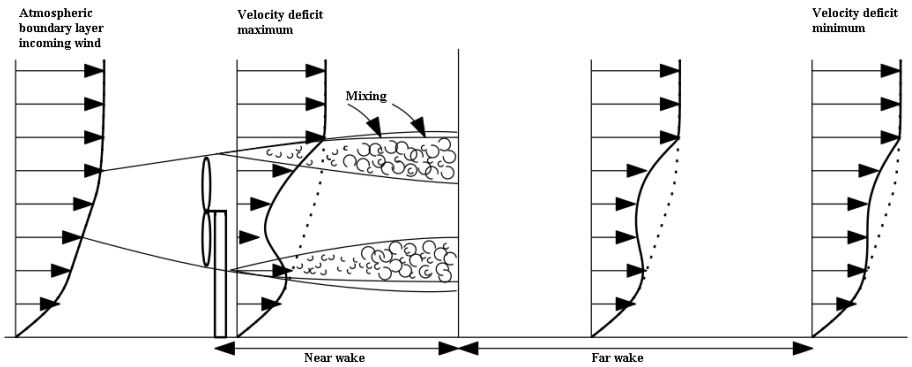

Figure 3.1: Near-wake and far-wake schematic of wind turbine placed in an atmospheric boundary layer.

The wind turbine wakes can be expressed by the incompressible Navier-Stokes equation, where the atmospheric flow of up- and downstream velocities range between 4 and 25 m/s. This is not valid for the blade tip region of the wind turbine. The governing equations in Einstein's notation and Cartesian coordinates are represented by equations 3.1 and 3.2. [16]

$$\frac{\partial u_j}{\partial x_j} = 0 \tag{3.1}$$

$$\frac{\partial u_i}{\partial t} + u_j \frac{\partial u_i}{\partial_j} = -\frac{1}{\rho}\frac{\partial P}{\partial x_i} + \frac{\partial}{\partial x_j}(2vS_{ij}) + f_i \tag{3.2}$$

Where u is the velocity, x the position vector, P is the pressure, ρ the fluid density, v is the kinematic viscosity, t is the time, i, j are the directional components, $f_i = \frac{F_i}{\rho}$ is the external body force and S_{ij} is the strain rate tensor defined as shown in equation 3.3.

$$S_{ij} = \frac{1}{2}\left(\frac{\partial u_i}{\partial x_j} + \frac{\partial u_j}{\partial x_i}\right) \tag{3.3}$$

Simplifications in both fluid and blade modelling are needed, due to equation 3.2 includes a non-linear convective term, $u_j \frac{\partial u_i}{\partial x_j}$. This is one of the main reasons an large number of turbulence models exists. [16]

3.2 Wake Models

There are many different wake models. Some of the wake models' main focus is to calculate near-wake and others focus on far-wake. In this project, the focus will be on far-wake kinematic models and will therefore be the focus in this chapter. Figure 3.2 shows a chart of well known and frequently used far-wake kinematic models, which will be the focus in this project. There are also far-wake field models which include the Eddy Viscosity model, Deep-Array model, and RANS model to name a few.

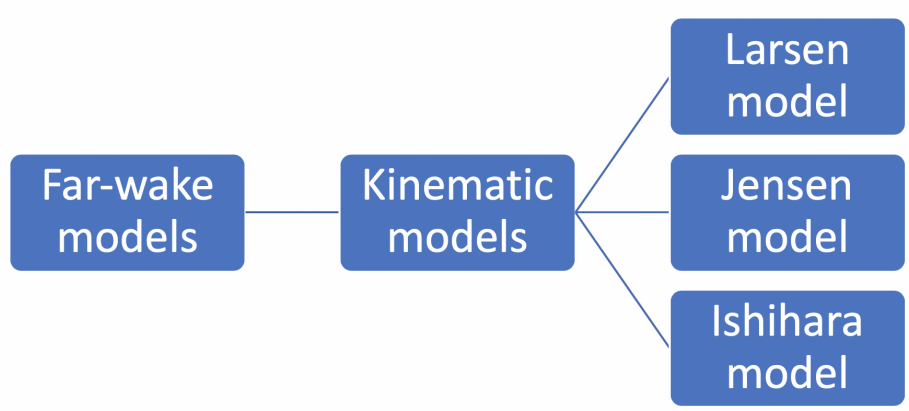

Figure 3.2: Flow chart showing different types of far-wake models

3.2.1 Jensen's Wake Model

The Jensen model is one of the oldest wake models and was originally developed by N.O. Jensen in 1983. [25] The concept of the model is simple and uses linearly expanding wake with a velocity deficit that is dependent on the distance behind the rotor. When Jensen created the model, he treated the wake behind the turbine as a turbulent wake that ignores the contribution of vortex shedding which is only significant in near-wake. If the near-region right behind the wind turbine is neglected, the wake behind the wind generator can be treated as turbulent. In the model, assumptions are made that the wake is turbulent, and the effects of tip vortices are neglected. This results in the model only being applicable for far-wake modeling. [25, 15]

There are two different types of the Jensen wake model. The Jensen single wake model and Jensen multiple wake model. The single wake model only looks at the wake from one wind turbine, i.e. the wake that can affect a wind turbine from other wind turbines is not taken into account. In the model the single wake is derived by conserving momentum across a control volume in the wind turbine's wake. On the other hand, the multiple wake model takes into account multiple turbines in a wind farm, or even from neighboring wind farms, where the wake from multiple wind turbines may affect the turbine under investigation. [15]

For the Jensen single wake model, the law of conservation of momentum applies, that is the radius of the wake behind the turbine expands linearly concerning the downwind distance. The law of conservation of momentum for wind turbines is shown in equation 3.4.[26]

$$\pi r_0^2 v_w + \pi(r^2 - r_0^2)v_0 = \pi^2 v_w \tag{3.4}$$

Where v_0 is the free-stream wind velocity, r_0 is the rotor radius of the wind turbine, r is the wake radius and v_w is the wake velocity. Betz theory shown in equation 3.5, it is used to see the relationship of the downstream velocity, which is represented by equation 3.4. [27]

$$v = (1 - 2a)v_0 \tag{3.5}$$

Where a is the axial flow induction coefficient, also known as induction factor. In the Jensen wake model, it is assumed that the wake downstream expands linearly. The radius of the area formed is estimated by using equation 3.6.

$$R_W = \frac{D(1 + 2\alpha x)}{2} \tag{3.6}$$

Where D is the rotor diameter of the wind turbine and R_W is the radius of the expanding wake. α, known as the decay constant, determines how quickly the wake expands with distance or describes the growth of the wake width. The decay constant has a default value of 0,075 in most land cases and a value of 0,04 for offshore applications. This can be calculated by using equation 3.7. [25]

$$\alpha = \frac{0,5}{ln\left(\frac{h}{z_0}\right)} \tag{3.7}$$

Where h is the wind turbines hub height and z_0 is the surface roughness of the wind farm. Equation 3.8 shows the wind velocity inside the single turbine wake area. This is the basics of Jensen's single wake model. As described before the Jensen wake model is for evaluating far-wake of 3-5D on-shore and 6-8D off-shore. This means that the velocity function is not accurate in the near wake regime. [28]

$$v_1 = v_0 + v_0(\sqrt{1 - C_T} - 1)\left(\frac{r_D}{r}\right)^2 \tag{3.8}$$

Equation 3.9 displays the velocity in the fully developed wake.

$$v_1 = v_0\left[1 - \frac{1 - \sqrt{1 - C_T}}{(1 + 2\alpha s)^2}\right]\pi r^2 \tag{3.9}$$

Where the wake radius r and the velocity v_1 are both dependent on downstream distance x_d, giving $s = x_d/2r$. C_T is the thrust coefficient of the upwind turbine. Since the velocity in the wake is constant for a given downstream distance, the shape of the velocity profile is called "hat-shaped". Located at s=0 right behind the rotor the velocity in the wake is expressed with equation 3.10. This means that because of the simplification in the Jensen wake model the thrust coefficient of the rotor needs to be smaller than one. [15]

$$u|_{s=0} = U_\infty\sqrt{1 - C_T} \tag{3.10}$$

The concept for the Jensen single wake model discussed above can be seen in figure 3.3.

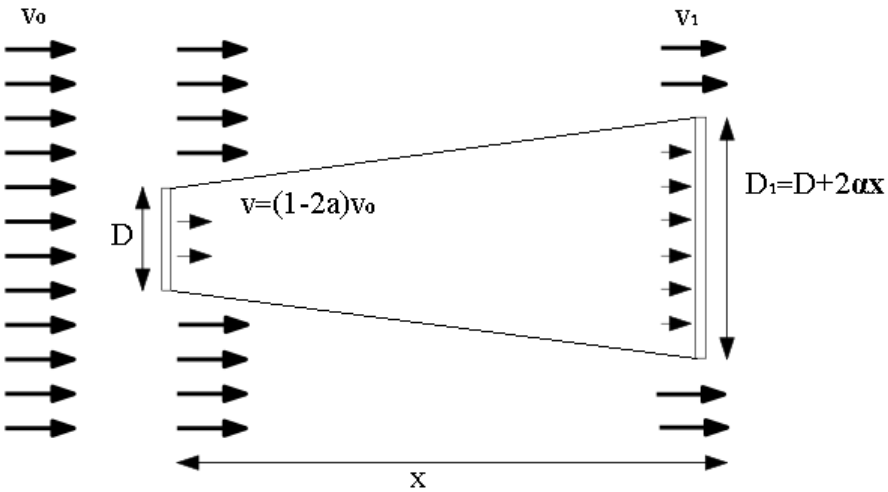

Figure 3.3: Jensen's single wake model

When looking at multiple wake effects with the Jensen wake model, the turbine in question is

facing multiple wake effects from upstream wind turbines. The resulting velocity v_i is given by equation 3.11. The equation shows that the sum of the kinetic energy deficits of each wake, with the kinematic energy deficit of the mixed wake at any given point. [15]

$$v_i = v_0 \left[1 - \sqrt{\sum_{i=1}^{Nt} \left(1 - \frac{v_i}{v_0} \right)^2} \right] \tag{3.11}$$

When looking at multiple wakes that can affect a wind turbine, partial shadowing is something that needs to be taken into account. This is when a wind turbine casts a shadow area on the upstream wind turbine. There are four different shadow conditions, complete shadowing, quasi complete shadowing, partial shadowing, and no shadowing. The shadowing is measured by the degree of overlap between the area of the turbine experiencing shadowing A_0 and the area spanned by the wake shadow $A_{shadow,i}$. The area of the turbine affected by the shadowing can be calculated, see equation 3.12, but only if all the wind turbines in the wind farm have the same diameter. [15]

$$A_{shadow,i} = [r_i(x_{ij})]^2 \cos^{-1}\left(\frac{L_{ij}}{r_i(x_{ij})} \right) + r_0^2 \cos^{-1}\left(\frac{d_{ij} - Lij}{r_i(x_{ij})} \right) - d_{ij} z_{ij} \tag{3.12}$$

Where x_{ij} is the distance between an upstream wind turbine i and a downstream wind turbine j. The radius of the wake behind the upstream wind turbine is represented with $r_i(x_{ij})$. d_{ij} is the distance between the centers of the downstream turbine and the center of the wake effect, which is $(r_i(x_{ij} + r_0))$. [15]

3.2.2 Larsen Wake Model

There are two versions of the Larsen wake model. The early version dating back to 1988 and the later version which is from 2009. The main difference between the early and later versions of the Larsen wake model is the boundary conditions and the wind farm approach. The earlier version of the model only took into account single wake cases, but not multiple wake cases. In the later version, the first boundary condition is defined at the rotor plane and the second one is defined at a fixed frame of reference placed at a distance 9,6D downstream. In the earlier version of the model, there was also a second-order approximation that was neglected in the later version. The wake radius and velocity deficit resulting from the updated boundary conditions are shown in equation 3.13. [29]

$$\begin{gathered} r_w(x,r) = \left(\tfrac{35}{2\pi}\right)^{\frac{1}{5}} \left(3c_1^2\right)^{\frac{1}{5}} \left(C_T A(x+x_0)\right)^{\frac{1}{3}}, \\ u_x(x,r) = -\tfrac{U_\infty}{9} \left(C_T A(x+x_0)^{-2}\right)^{\frac{1}{3}} \\ \left\{ r^{\frac{3}{2}} (3c_1^2 A(x+x_0))^{-\frac{1}{2}} - \left(\tfrac{35}{2\pi}\right)^{\frac{3}{10}} (3c_1^2 f)^{-\frac{1}{5}} \right\}^2 \end{gathered} \tag{3.13}$$

Where c_1, x_0 and d_1 are as shown in equations 3.14-3.16.

$$c_1 = \left(\frac{105}{2\pi}\right)^{-\frac{1}{2}} \left(\frac{d_1 D}{2}\right)^{\frac{5}{2}} (C_T A x_0)^{-\frac{5}{6}} \tag{3.14}$$

$$x_0 = \frac{9,6D}{\left(\frac{2R9.6D}{d_1 D}\right)^3 - 1} \tag{3.15}$$

$$d_1 = \sqrt{\frac{1 + 1/\sqrt{1 - C_T}}{2}} \tag{3.16}$$

Where $R_{9,6D}$ is the wake radius at 9,6D, which is analytically calculated and expressed using atmospheric turbulence intensity I_a as shown in equation 3.17.

$$R_{9,6D} = a_1 \exp\left(a_2 C_T^2 + a_3 C_T + a_4\right)(b_1 I_a + 1)D \tag{3.17}$$

For the wind farm approach there are two different methods for calculating the inflow speed, which is the geometric also known as linear , shown in equation 3.18 and momentum balance represented by equation 3.19.

$$U_\infty = \overline{U} = \frac{1}{A}\int_A U dA \tag{3.18}$$

$$\overline{U} = \sqrt{\frac{1}{A}\int_A U^2 dA} \tag{3.19}$$

Where U is the incoming ambient velocity modeled with logarithmic wind profile. The velocity in the wind farm is calculated using a linear averaging shown in equation 3.20.

$$\overline{U}_m = \overline{U} - \sum_{i=1, R_i \leq r_{0_i}+R}^{M} u_{x_i} \tag{3.20}$$

Where M is the number of upstream rotors that generate wakes affecting the rotor. But for the non-linear approach the decomposition of $\overline{U}_m$ can not be calculated linearly and therefore is represented by equation 3.21.

$$\overline{U} = \sqrt{\frac{1}{A}\int_A \left(\overline{U} - \sum_{i=1, R_i \leq r_{0_i}+R}^{M} u_{x_i}\right)^2 dA} \tag{3.21}$$

The 4-point Gauss integration method is used to solve equations 3.20 and 3.21. Also for both equations, the multiple wake effects are superposed using the linear sum. [29, 16]

3.2.3 Ishihara Wake Model

The Ishihara wake model was developed by Ishihara *et. al* [30] from the University of Tokyo in 2004. To develop the wake model, wind tunnel data was used from a model a Mitsubishi wind turbine. The model was designed to take into account the effect of turbulence on the wake recovery. It is not constant and depends on the atmospheric and rotor generated turbulence and also the downstream distance from the wind turbine. Therefore, the wake recovery is more dependent on the turbine-generated turbulence. A part that differentiates the Ishihara wake model from the Jensen wake model, is that in the Jensen wake model, a top hat velocity profile is assumed in the wake, but a Gaussian profile is used in the Ishihara wake model. It also predicts the wake for any ambient turbulence and thrust coefficient. The velocity deficit in the wake of the turbine is given by the equations 3.22-3.25. [13]

$$\frac{u_1(x,r)}{U_0} = \frac{C_t^{\frac{1}{2}}}{32}\left(\frac{1.666}{k_1}\right)^2\left(\frac{x}{d}\right)^{-p}\exp\left(\frac{-r^2}{b^2}\right) \tag{3.22}$$

$$b(x) = \frac{k_1 C_t^{\frac{1}{4}}}{0.833} d^{1-\frac{p}{2}} x^{\frac{p}{2}} \tag{3.23}$$

$$p = k_2(I_a + I_w) \tag{3.24}$$

$$I_w = k_3 \frac{C_t}{max(I_a, 0.03)}\left(1 - \exp\left(-4\left(\frac{x}{10d}\right)^2\right)\right) \tag{3.25}$$

Where in equations 3.23-3.25 the following constants are $k_1 = 0.27$, $k_2 = 6.0$ and $k_3 = 0.004$

3.3 Weibull Distribution

Weibull distribution has attracted attention for the last half a century in the field of statistical analysis on theory, method, and in other fields of statistics. Alongside the normal, exponential distributions, the Weibull distribution is the most popular statistical model today. The Weibull distribution has caught attention from theory-oriented statisticians, due to its unique features and its ability to fit data from various fields. From life science, meteorological and economical data to engineering science to name a few. In the Weibull distribution, there are two important functions, the cumulative distribution function and the Weibull's probability density function.

3.3.1 Cumulative Distribution Function

The cumulative distribution function is the integration of the Weibull density function also known as the Weibull function. It is cumulative of the relative frequency in every velocity interval. The equation for the Weibull function is given by equation 3.26. [31]

$$F(v) = \int_0^v f(v')d(v') \tag{3.26}$$

Which also can be written as equation 3.27.

$$F(v) = 1 - e^{-\left(\frac{v}{c}\right)^k} \tag{3.27}$$

3.3.2 Weibull's Probability Density Function

The equation for Weibull's probability density function is given by equation 3.28. The purpose of this function is to estimate the distribution of the subject under analysis, that way it is possible to see the shape of it when plotting it. [31]

$$f(v) = \frac{dF(v)}{dv} = \left[\frac{k}{c}\right]\left[\frac{v}{c}\right]^{k-1} \times e^{-\left(\frac{v}{c}\right)^k} \tag{3.28}$$

3.4 WindSim

WindSim is a Wind Farm Design Tool (WFDT). It is used to optimize the energy production of the wind farm while keeping the loads affecting the wind turbines within acceptable limits. This is done by calculating numerical wind fields over a digitalized terrain, this is also called micro-siting. WindSim uses a modular approach using six modules to complete the micro-siting. These six modules are Terrain, Wind Fields, Objects, Results, Wind Resources and Energy. [32]

In the terrain module, the numerical model is established on height and roughness. In the wind fields module, the numerical wind fields are calculated. In the objects module, the wind turbines are placed and the climatology data is processed for the location that is being analyzed. Also, noise calculations for the area are done in this module. The results module analyses the numerical wind fields. In the wind resource module, the numerical wind fields and climatology data are coupled together with statistics to make a wind resource map. In the energy module, the results from the wind resource module are used to determine the annual energy production, as well as the wake losses are calculated in this module. [32]

Below, only the functions from WindSim relevant to this project will be theoretically explained.

3.4.1 Roughness

The roughness is determined in the terrain module. To find the roughness height WindSim uses the log-law to calculate it. The log-law is shown in equation 3.29. [33]

$$\frac{u}{U_T} = \frac{1}{\kappa} ln\left(\frac{z}{z_0}\right) \tag{3.29}$$

Where u is the wind velocity, U_T is the friction velocity and is defined by equation 3.30. T_0

is the shear stress, ρ the air density. κ is the Von Karman constant which is 0,435, z is the coordinate in the vertical direction and z_0 is the roughness height.

$$U_T = \frac{T_0}{\rho}^{0,5} \tag{3.30}$$

3.4.2 Generation of the wind fields

The wind fields are calculated in the wind fields module. The wind fields are calculated by using the Reynolds Averaged Navier-Stokes equations also known as RANS equations. Where the standard k-epsilon model is applied as turbulence closure. WindSim uses PHENICS to solve the RANS equations. The flow variables that are solved are pressure (P1), velocity components (U1,V1,W1), turbulent kinetic energy (KE), and turbulent dissipation rate (EP). [33, 34]

3.4.3 Turbulence model

The wind fields module also contains the turbulence module. The default turbulence model in WindSim is the standard $k-\varepsilon$. The $k-\varepsilon$ model is in the Eddy Viscosity Model Family. For high turbulent Reynolds numbers, the standard form of the $k-\varepsilon$ is defined by equations 3.31-3.33. [33, 34]

$$(\rho\, K), t + \left(\rho\, U i K - \frac{\rho\, v_t}{PRT(K)} K, i\right), i = \rho\,(PK - \varepsilon) \tag{3.31}$$

$$(\rho\, \varepsilon), t + \left(\rho\, U i \varepsilon - \frac{\rho\, v_t}{PRT(\varepsilon)} \varepsilon, i\right), i = \frac{\rho\varepsilon}{k}(C1\, PK - C2\, \varepsilon) \tag{3.32}$$

$$v_t = C_\mu \frac{K^2}{\varepsilon} \tag{3.33}$$

Where K is the turbulent kinetic energy, ε is the dissipation rate, ρ is the fluid density, v_t is the turbulent kinematic viscosity and C_μ,$C1$,$C2$,$PRT(k)$ and $PRT(\varepsilon)$ are the model constants. Furthermore, t is denoting differentiation concerning the time and i is denoting differentiation with respect to the distance. [33, 34]

3.4.4 Actuator disc

The actuator disk calculations are also in the wind fields module. The cells that are covering an area A of the "disc" of the wind turbine. The area of the circle, the blades of the wind turbine make. Exert forces directed against the wind in the axial direction. The force thrust F_i is defined by equation 3.34. [33, 35]

$$F_i = C_T(U_{1,i}) 0.5 \rho \left(\frac{U_{1,i}}{1-\alpha_i}\right)^2 A_i \tag{3.34}$$

Where $U_{1,i}$ is the velocity of the flow in at the i-th cell. α_i is the axial induction factor calculated for each cell. A_i is the surface area of the cell facing the undisturbed wind flow direction. $C_T(U_{1,i})$ is a modified thrust coefficient dependent on the velocity at the disc $U_{1,i}$ and ρ is the air density. C_T is responsible for the first wind turbine of the row but not the downstream wind turbines where the airflow is disturbed, therefore the velocity of the disc is needed since C_T is a function of U_1. This function is defined with the 1D momentum theory by combining the definitions of the thrust coefficient and the axial induction factor. See equation 3.35. [33, 35]

$$C_T = 4\alpha(1-\alpha) \tag{3.35}$$

$$U_1 = (1-\alpha)U_\infty \tag{3.36}$$

From equations 3.35 and 3.36, equation 3.37 is obtained.

$$U_1 = U_\infty \left(1 - 0.5\left(1 - \sqrt{1 - C_T(U_\infty)}\right)\right) \tag{3.37}$$

The power production is calculated by finding the average induction factor over the disc $\overline{a} = \frac{1}{N\sum \alpha_i}$. For each velocity over the disc an undisturbed wind velocity v_0 is calculated with equation 3.38. [33, 35]

$$v_0 = \frac{U_{1,i}}{1-\overline{a}} \tag{3.38}$$

For each undisturbed wind velocity the power is found by using the power curve of the wind turbine, then they are averaged over the disc. [33, 35]

3.4.5 Wake Models

The wake effect is calculated in the wind resources module. There are three wake models to choose from in WindSim, they are all analytical methods, which are often as they are more simple and less computationally demanding than CFD based methods. All the wake models are single wake models calculating the normalized velocity deficit (δV). All the models are rotational along the x-axis, which implies that the reduced wakes will be calculated at hub height. [33]

Model 1 is based on the Jensen model and gives a simple linear expansion of the wake. The wake effect for model 1 is given by the deficit theory displayed in equation 3.39. [33, 7]

$$\delta V = \frac{1 - \sqrt{1 - C_T}}{\left(1 + \left(\frac{2kx}{D}\right)\right)^2} \tag{3.39}$$

Where C_T is the thrust coefficient, D is the rotor diameter and k is the wake decay factor. The equation for the wake decay factor is displayed in equation 3.40.

$$k = \frac{A}{ln\left(\frac{h}{z_0}\right)} \tag{3.40}$$

A is a constant of 0,5, h is the hub height in meters and z_0 is the roughness height in meters.

Model 2 is based on the Larsen model. It is defined by the turbulent boundary layer equations and a similarity assumption shown in equation 3.41. [33, 36]

$$\delta V = \frac{1}{9}\left(C_T A_r x^{-2}\right)^{1/3}\left(r^{3/2}\left(3C_1^2 C_T A_r x\right)^{-1/2} - \left(\frac{35}{2\pi}\right)^{3/10}\left(3C_1^2\right)^{-1/5}\right)^2 \tag{3.41}$$

Where I_a is the ambient turbulent intensity at hub height and A_r,C_1,x_0,R_{95} and R_{nb} are given by equations 3.42-3.46 respectively.

$$A_r = \frac{\pi D^2}{4} \tag{3.42}$$

$$C_1 = \left(\frac{D}{2}\right)^{5/2}\left(C_T A_r x_0\right)^{-5/6} \tag{3.43}$$

$$x_0 = \frac{9,5D}{\left(\frac{2R_{95}}{D}\right)^3} - 1 \tag{3.44}$$

$$R_{95} = 0,5\left(R_{nb} + min(h, R_{nb})\right) \tag{3.45}$$

$$R_{nb} = max(1,08D, 1,08D + 21,7D(I_a - 0,05)) \tag{3.46}$$

Model 3 is based on the Ishihara wake model and is defined by a turbulent depending rate of wake expansion, shown in equation 3.47. [33, 30]

$$\delta V = \frac{C_T^{1/2}}{32}\left(\frac{1,666}{k_1}\right)^2\left(\frac{x}{D}\right)^{-p}\exp\frac{-r^2}{b^2} \tag{3.47}$$

Where b, p and I_W are defined by equations 3.48-3.50 respectively.

$$b = k_1\frac{C_T^{1/4}}{0,833}D^{(1-(p/2))}x^{p/2} \tag{3.48}$$

$$p = k_2(I_a + I_W) \tag{3.49}$$

$$I_W = k_3\left(\frac{C_T}{max(I_a, 0,03)}\right)\left(1 - \exp\left(-4\left(\frac{x}{10D}\right)^2\right)\right) \tag{3.50}$$

Where the constants $k_1 = 0,27$, $k_2 = 6,00$ and $k_3 = 0,004$.

The definition of multiple wake is when more than one turbine influences the velocity at the considered location. Then, the velocity deficits calculated by the single wake equations are combined to obtain an equivalent wake deficit. WindSim uses the linear superposition of the wake deficits which is represented in equation 3.51. WindSim also uses the squared root of the sum of the squares which is shown in equation 3.52. [33]

$$\delta v = \sum \delta v_i \tag{3.51}$$

$$\delta v = \sqrt{\sum \delta v_i^2} \tag{3.52}$$

4 | Methods

4.1 Wind Farm Description

The wind farm that is being analyzed in this project is the Wind R&D Park located in North Cape on Prince Edward Island in Canada. The wind farm is owned by the Wind Energy Institute of Canada also known as WEICan. Figure 4.1 shows a map of Canada and the location of Prince Edward Island. The island is located near the border of Canada and the United States of America. The red box in the figure of the island shows where the wind farm is located on the island at North Cape. The wind turbines are located in the north-western part of the North Cape area.

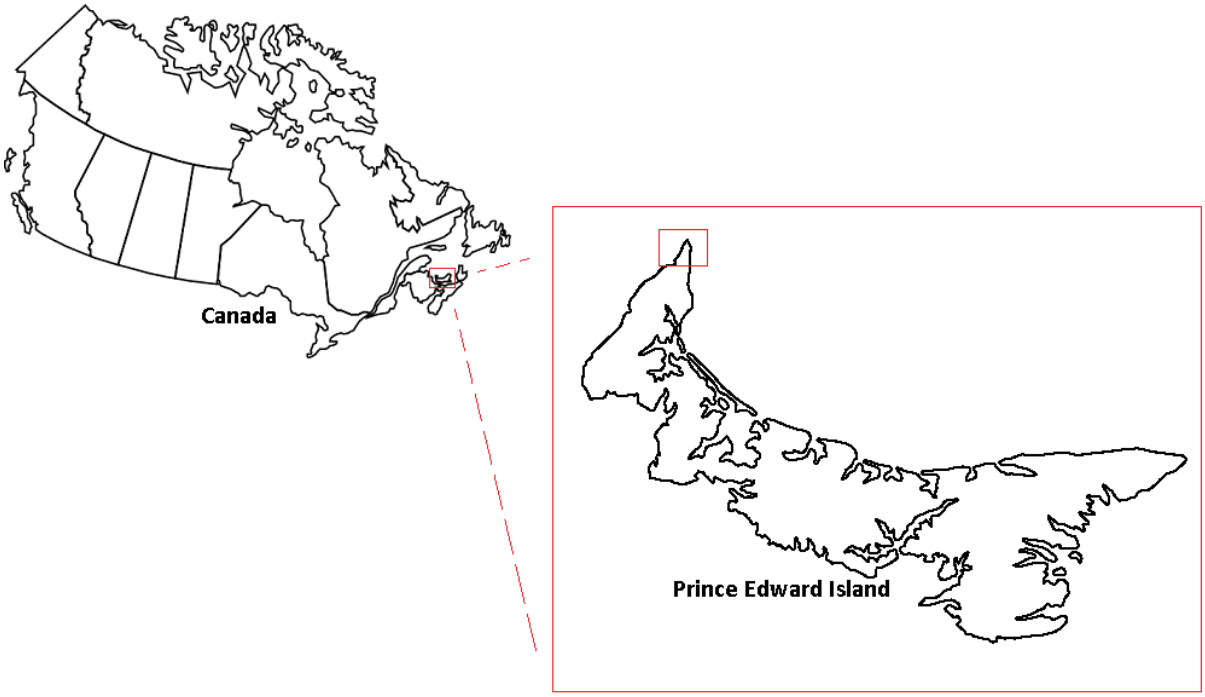

Figure 4.1: Map of Canada and Prince Edward Island.

A closer look at the wind farm is shown in figure 4.2, where the elevation of the terrain is displayed, the green and blue area of the figure is the ocean. The yellow and brown colors show different elevations of the terrain, where the lighter colors are lower elevation and the elevation increases as the colors get darker. There are five wind turbines in the wind farm. They are

represented by a triangle and the met tower is represented by a circle in figure 4.2. Turbine one is located furthest north, then come turbines two, three, and four respectively in a row after the first turbine. Turbine five is located furthest south and further inland than the other turbines. The meteorological (met) tower is located close to turbine five and that is why the circle and triangle look more like a rectangle in the figure since the markers are nearly on top of each other. The turbines' height above sea level is from 9,8-10,7 m, meaning they are all located at similar ground heights.

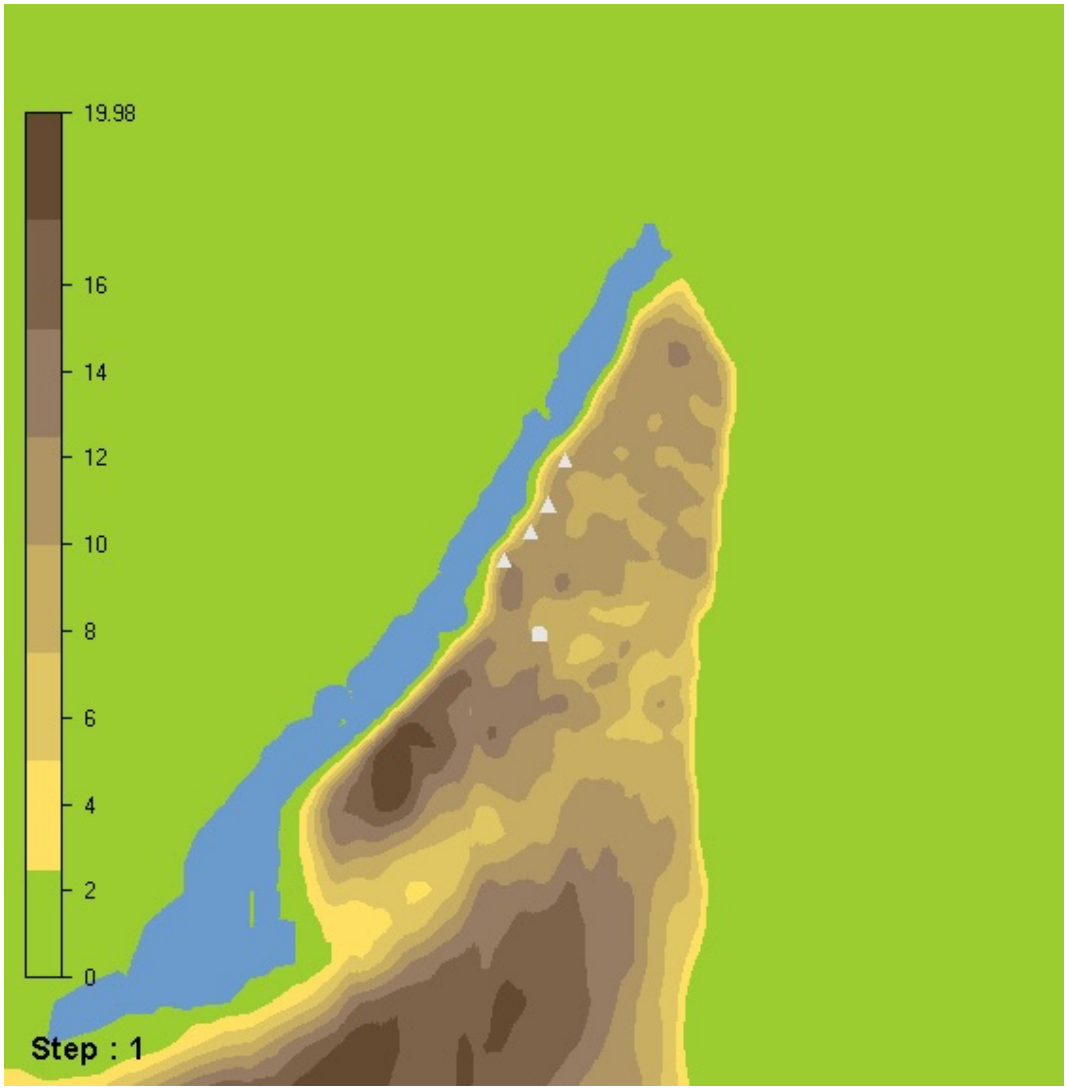

Figure 4.2: Elevation of the wind farms terrain and placements of the turbines and met tower.

Figure 4.3(a) shows the terrain roughness of the wind farm. Where the white and blue area is the ocean. The red and yellow colors show the roughness of the terrain, where the lighter colors have less roughness and the darker colors show more roughness. As can be seen, the area of the wind farm is fairly even. Showing the largest portion of the area having roughness between 0,6 and 0,667 displayed in a dark red color. In figure **??**(b) the wind rose for the wind farm can be seen for the years 2016-2019. As seen on the figure, westerly directions are the most dominant wind directions in the area. Furthermore they are also far higher in velocity that the wind coming from opposite directions.

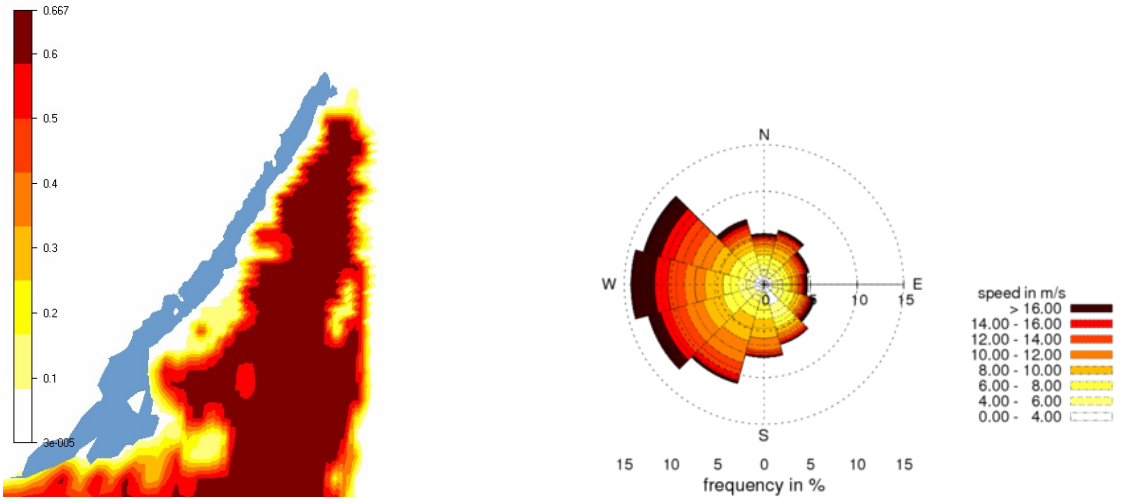

(a) Terrain roughness of the wind farm

(b) Wind rose for all velocity and directional bands

Figure 4.3: Where figure (a) shows the roughness of the wind farm's terrain. Figure (b) shows the wind rose for the wind farm, for all velocity and directional bands.

The wind farm consists of five 2MW wind turbines, which means the wind farm has a total installed capacity output of 10MW. The turbines are all of the type DeWind D9.2 with AB45 blades. Table 4.1 shows all the specifications of the wind turbines. The DeWind turbines include a synchronous generator coupled to the variable speed rotor through a hydraulic Voith WinDrive. As can be seen from figure 4.1 the wind turbines are placed by the sea. With the harsh coastal environment and cold weather, the wind turbines have an annual capacity factor above 45%. [37]

Table 4.1: Wind turbines specifications at the WEICan R&D Park.

Manufacturer	DeWind
Product name	D9.2
Blade name	AB45
Blade diameter	93 m
Hub height	80 m
Nominal power	2000 kW
Nominal power at wind speed	13 m/s
Cut-in wind speed	4 m/s
Cut-out wind speed at	25 m/s

4.2 Data

The power curve for the DeWind D9.2 turbines used in the wind farm is represented by figure 4.4. The power curve was obtained with an air density of $1.225 kg/m^3$. The main information from this power curve was stated in table 4.1. For the WindSim simulations a power curve document needed to be made so the program would know the capacity of the turbines, and their performance. The power curve document was made using the values displayed in figure 4.4. Where the first column of the sheet was the wind speed in [m/s] the second column was the power output in [kW] and the third column was the thrust coefficient. The thrust coefficient was not given with the power curve information that was provided by WEICan. Since the thrust coefficient was needed for the wake model calculations in WindSim, the thrust coefficient was obtained directly from the DeWind manufacturer. The thrust coefficient for the DeWind D9.2 2MW turbine couldn't be obtained, so the thrust coefficient from the DeWind D8 2MW turbine was used, which have similar values. WindSim has two types of setup for the power curve document. The setup needs to be exact so that the program can read the files. The types that WindSim has are named 450 and 470. 450 has no thrust coefficient information and 470 has thrust coefficient information. Since the thrust coefficient information was needed type 470 was used for this project.

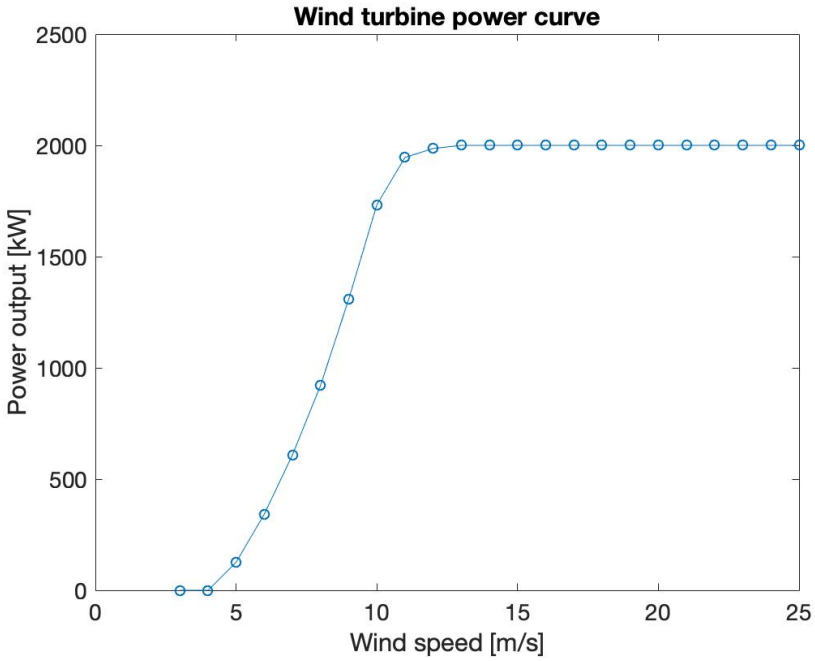

Figure 4.4: Power curve for the wind turbines.

The terrain and roughness maps were made in the Geographic information system (GIS) Global Mapper [38]. The coordinates of the wind farm were calculated by finding the middle of the wind farm. Global mapper takes the coordinates and makes an area that is 10 km in every direction from the coordinates and makes a file that contains the terrain and roughness information. This area is defined as the wind farm in this project.

To make the climatology files, the program Windographer was used [39]. To make the files the wind speed and wind direction were needed. Data from the Wind R&D Park was used in this project from the years 2016-2019. Data collected in the Wind R&D park, from the years 2016-2019 was used in the project's simulations. The wind speed and direction used to make the climatology file was taken from the met mast located in the wind farm near turbine five. The ultrasonic detector in the type of Sonic 3D from Thies Clima at 80 m height was used in this project to obtain the data.

Before the data could be used in Windographer, the data needed to be cleaned. The cleaning of the data was done by using Microsoft Excel, where all abnormal values were removed, including negative values. The values that were right before the wind speed reached a negative value or right after, were often out of place and therefore also removed. In 2017 there was a malfunction of all the sensors on the met mast. That means that there was no data from 01.04.2017 at 00:00 to 23.09.2017 at 11:30 in 2017. To make sure the data was reliable the data was plotted and random values that were out of place were removed as well. The meteorological data for all four years was combined into one .csv file, which was used as a base for the .csv files needed for the project.

Three .csv files were made from the file mentioned. One that only included data for a velocity band of 3-7 m/s, another that only included data for the velocity band 7-11 m/s, and lastly a file for the velocity band 11-15 m/s was made. These were the velocity bands that the wake effect was analysed for.

The directional band that was focused on in this project is from $230° - 320°$. As already shown in figure 4.3(b) in chapter 4.1 the dominant wind direction in the wind farm is from the west. The direction for west equals 270°, and as can also be seen the most dominant wind is in the space of approximately $225° - 315°$. The directional bands were simulated for every 10° in this project the directions chosen were rounded up to $230° - 320°$. Thus, for each velocity band, 9 .csv files were needed with the relevant parameters. Making a total of 27 .csv files. Climatology files were made for each of the .csv files, including the main file. Giving a total of 28 climatology files. As mentioned before the climatology files were made in Windographer. Table 4.2 shows the specifications for making the climatology files in Windographer.

Table 4.2: Windographer specifications for the climatology files

Time step	10 minutes
Height	80 meters
Direction sectors	36
Speed bin size	0,5 m/s
File type	WWS

Meteorological data from the met mast was recorded every ten minutes, making it the time step used in the project. The height for the wind speed and wind direction was set to 80 meters since the met mast that the data is from is at that height. The latitude, longitude, and elevation of the site were added into the files as well. WindSim was chosen in Windographer since that is the

simulation program that was used and the climatology file made in the type wws, which is the file type that WindSim requires. The speed bin size determines the gap between values of the speed, 0,5 m/s was chosen since it is the lowest gap Windographer offers and it is important to keep the gap as small as possible since the velocity bands that were analyzed are small. Lastly, the sectors were set to 36. That number was chosen due to each csv file contains 10° of data, which means that Windographer and WindSim need to look at all 36 sectors to perform the calculations for all the directional bands.

4.3 WindSim Simulations

As mentioned in chapter 3.4 WindSim is built of six modules. The settings that were applied to WindSim for this project are as shown in table 4.3.

Table 4.3: WindSim specifications for the simulations

Maximum number of cells in xy direction	500.000
Maximum number of cells in z direction	60
Number of sectors	36
Turbulence model	Standard k-epsilon
Wake model	Model 1/2/3
Influence range of wake	2:10 rotor diameter
Angle of turbines	270°
Rotor diameter	93m
Hub height	80m

By setting the maximum number of cells in the xy direction to 500.000, the number of cells for the terrain was at 496.800. The maximum number of cells in the xy direction of 500.000, since it was believed to give high enough accuracy for the simulations for this terrain, since the terrain is mostly flat and has similar overall roughness. This is shown in figure 4.5(a), where the refinement area for the wind farm can also be seen. The maximum number of cells in z direction was set to 60 for the same reasons as for the xy direction. In figure 4.5(b) the refinement for the z direction can be seen.

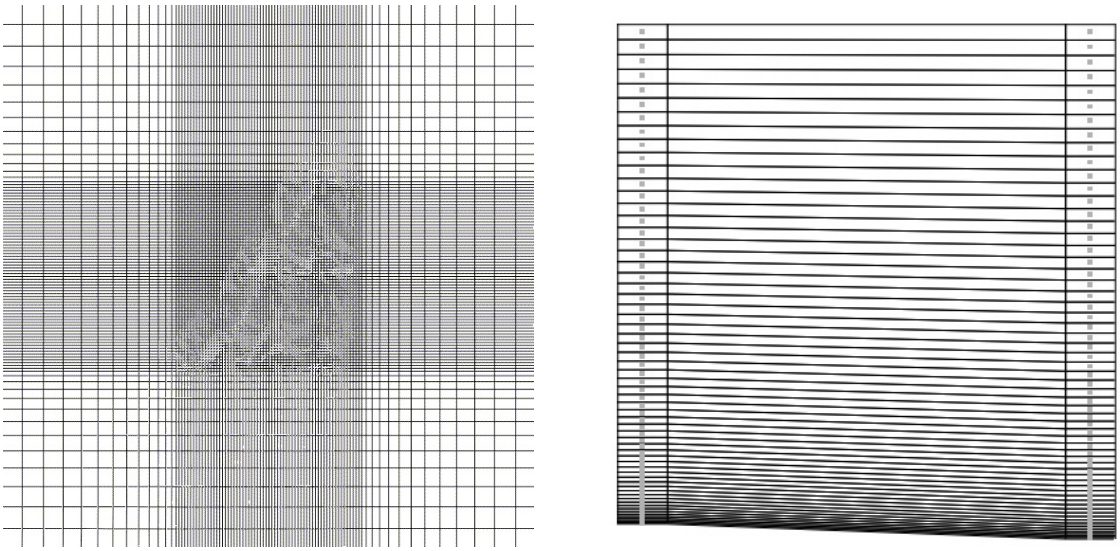

(a) Refinement area in the xy direction

(b) Refinement of the z direction

Figure 4.5: Where figure(a) shows the refinement area of the wind farm in xy direction. Figure(b) shows the refinement in the z direction

The number of sectors was chosen as 36 to be in accordance with the climatology les as described

in chapter 4.2. For every 10° of the wind directions interval the calculations must be performed for the most accurate result. The turbulence model that was chosen for the project is the standard k-epsilon turbulence model, which is the default turbulence model for WindSim. The three wake models that WindSim offers were compared to each other in this project. The far-wake is of more interest than near-wake. Due to this, the influence range of the wake was set from 2 rotor diameters to 10 rotor diameters. The reason for choosing to start at 2 rotor diameters and not 1 is due to a warning that occurred when the Ishihara wake model was running, that the near wakes could not be calculated. Since far-wake is of more interest, and in order to prevent any warnings, which might have affected the outcome during the simulations, the minimum influence range was increased to 2 rotor diameters The angle of the wind direction that the turbines was facing was set to 270°, which is west. The hub height and the height of the measurements are set to 80m since that is the hub height of the wind turbines in the wind park.

Since the goal of the project was to look at the wake at different velocity and directional bands the simulations needed to be concluded for every climatology file individually to get the results needed to do the analysis, or 27 simulations in WindSim. In addition, a simulation was done for the climatology file from the main .csv file to be able to get the wind rose in figure 4.3(b) and detect the main wind direction and behavior of the wind for the site.

4.4 Processing of the Results

The average energy production (AEP) with wake loss was documented for all the simulations performed in WindSim. To compare the measured power production with the simulated power production, the data from each turbine, including wind speed and power production was used. Since the simulations were performed at every 10° the direction of the wind was also needed, since each turbine didn't have the directional information of the wind, the wind direction from the met mast was used. Both the met mast and wind turbine data were at 10-minute intervals. The data was assembled so that the time intervals lined up. It was then cleaned as previously described and split into the corresponding velocity and directional bands. Making a total of 135 files of power production data.

To compare the simulated results against the measured data, the measured data needed to be converted to one value per wind turbine. That was done by finding the average power production for each wind turbine, which was then normalized, making wind turbine one the turbine that the others were compared to as equation 4.1 shows.

$$P_N = \frac{P_{Ei}}{P_{E1}} \tag{4.1}$$

Where P_N is the normalized power, P_{E1} is the power production for wind turbine one, and P_{Ei} is the power production at wind turbine number i. The simulated results from the wake models were normalized the same way. On the other hand, showing only the average power production of individual wind turbines is not accurate enough. In order to show the whole

expanse of the power production the standard deviation of each wind turbine was calculated by first normalizing all the data from the wind turbines by using equation 4.2.

$$P_N = \frac{P_{Emax}}{P_E} \tag{4.2}$$

Where P_N is the normalized power for each value, P_{Emax} is the maximum power value for each wind turbine for the velocity and directional bands chosen. P_E is the power production value that is being normalized. The normalization for the standard deviation was calculated according to equation 4.2 instead of 4.1 since the first value in the data can be high or low, this way the highest value is always one. Making the standard deviation between zero and one.

Subsequently the standard deviation was calculated from the normalized values using equation 4.3.

$$\sigma = \sqrt{\frac{\sum(x_i - \mu)^2}{N}} \tag{4.3}$$

Where σ is the standard deviation, x_i represents each value in the data, μ is the mean value of the data, and N is the number of values in the data set. The normalized power production for the measured data and the simulations were transferred into Matlab, along with the normalized standard deviation. Where the graphs for all the 27 cases were made. This was done to show the range of data for all the turbines, and not only the average value. The values used to create the graphs in Matlab, both from the simulations and for the error calculations, are displayed in Appendix A. Error calculations were also completed. The error matrices used were root mean square error (RMSE), normalized root mean square error (NRMSE), and mean absolute error (MAE). To calculate the RMSE equation 4.4, where obs represents the observed or measured data and sim represents the simulated data.

$$RMSE = \sqrt{\frac{\sum obs - sim}{(\sum obs - sim)^2}} \tag{4.4}$$

To find the NRMSE equation 4.5 was used. Where $\overline{obs}$ is the average value of the observed data.

$$NRMSE = \frac{RMSE}{\overline{obs}} \tag{4.5}$$

To calculate the MAE equation 4.6 was used.

$$MAE = \frac{\sum |(obs - sim)^2|}{N} \tag{4.6}$$

5 | Results

In this chapter the normalized result of the annual power production, with wake losses from the WindSim simulations, alongside the production data of the wind farm will be shown. The results will be displayed for all the velocity and directional bands. Due to an non-disclosure agreement (NDA) with WEICan the normalized values were used for the simulations and the error calculations. All the graphs have different scale at the y-axis to be able to see the behaviour of the wake as closely as possible.

5.1 Velocity band 3-7m/s

Figure 5.1 displays the results for the simulations for the directional band $230° - 240°$. As shown for the simulated values, turbine two has higher wake loss than turbine one. The Ishihara model is showing the smallest wake loss and is closest to the measured data, the Jensen model is showing second smallest wake loss, and the Larsen wake model is showing the largest wake loss for turbine two. Turbine three is experiencing the largest wake loss, where the Larsen model shows the smallest wake loss and is the closest to the measured data, then the Ishihara model, and showing the largest wake loss is the Jensen model. Turbine four is experiencing the least amount of wake loss, and as can be seen, all the wake models were showing the same result for turbine four. Turbine five shows the second largest amount of wake loss, all the wake models are showing the same result. The measured data does not show the same behaviour of wake loss for each turbine as the simulated values for this directional band. Turbine two shows has the closest simulated value to the measured value, then turbine four, both turbines three and five are showing large deviation from the measured data.

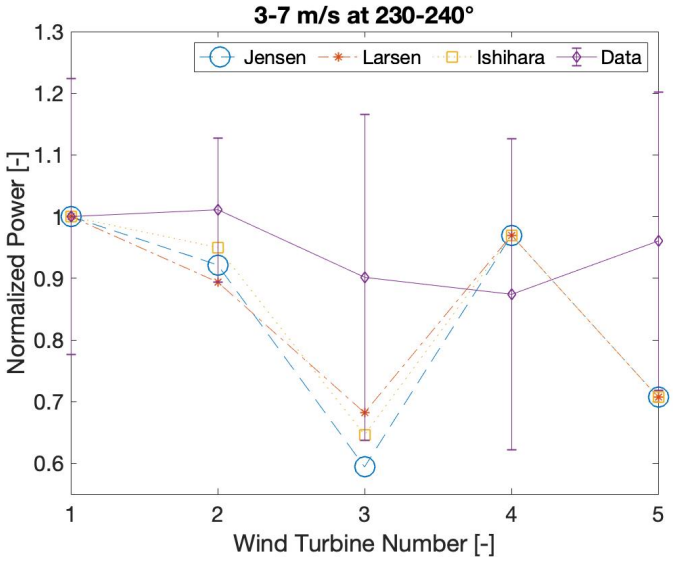

Figure 5.1: Simulated results compared with measured data for the velocity band 3-7 m/s and directions $230 - 240°$

Figure 5.2 displays the results for directional band $240° - 250°$. For the simulated values, turbine two and turbine one have similar wake loss. For turbines two, four, and five all the wake models are displaying the same results for each wind turbine. Turbine three is affected by slightly higher wake loss than turbine two, where the Larsen model is showing more wake loss than the other models, and is the closest to the measured data. The Ishihara and Jensen wake models show similar values though, the Ishihara model is showing slightly more wake loss than the Jensen model. Turbine four is being affected by the least amount of wake loss. Turbine five is being affected by the largest wake loss for this directional band. Turbine five is showing the largest difference between the simulated and measured values, followed by tribune four. Turbines three and two are showing similar difference.

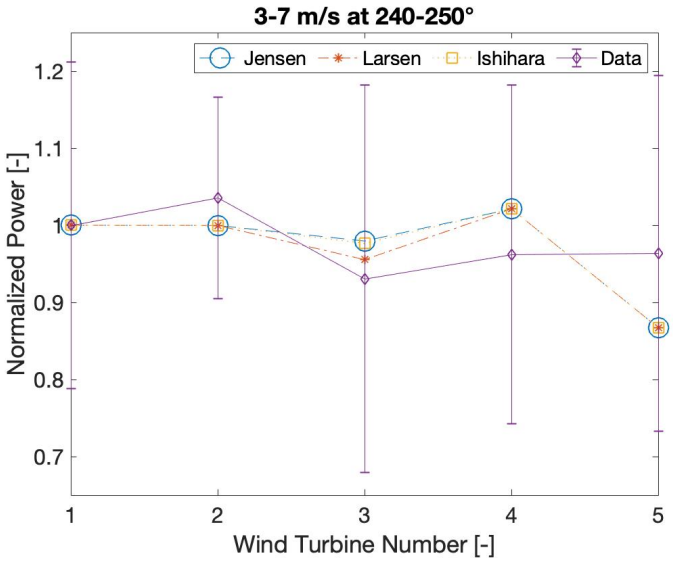

Figure 5.2: Simulated results compared with measured data for the velocity band 3-7 m/s and directions $240 - 250°$

Figure 5.3 displays the results for the directional band of $250° - 260°$. All the turbines are experiencing similar wake loss for the simulations. The simulated values are showing much lower wake loss than the measured data is showing. Furthermore, all the wake models are showing the same results for each turbines.

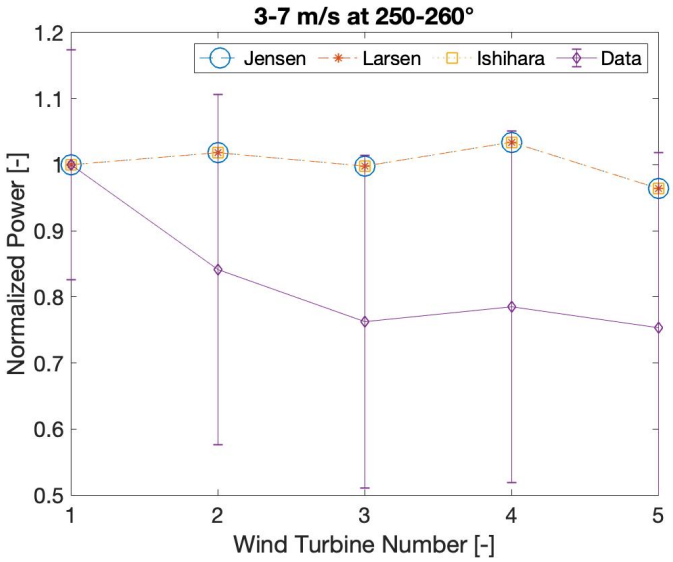

Figure 5.3: Simulated results compared with measured data for the velocity band 3-7 m/s and directions $250 - 260°$

Figure 5.4 displays the results for $260° - 270°$. The simulated values are closer to the measured data for this directional band than for figure 5.3. All the turbines are also showing similar wake losses for this directional band according to the measured and simulated values.

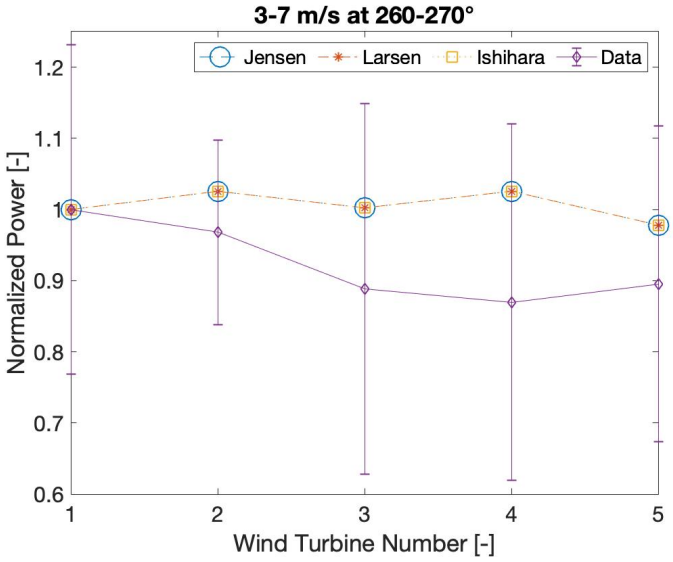

Figure 5.4: Simulated results compared with measured data for the velocity band 3-7 m/s and directions $260 - 270°$

Figure 5.5 displays the results for directional band $270° - 280°$. The gap between the measured and simulated values are narrower than in figure 5.5. Indicating that the accuracy of the sim-

ulations is getting better as the directional bands get higher. Turbines two and four show the largest deviation between the measured and simulated values.

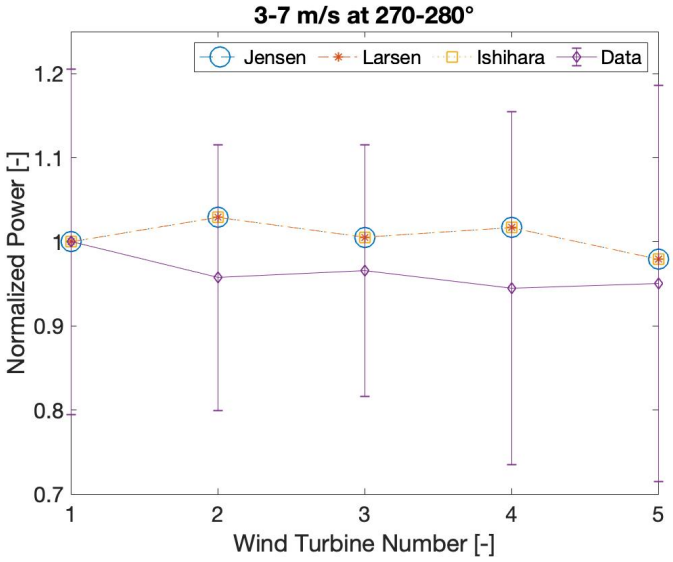

Figure 5.5: Simulated results compared with measured data for the velocity band 3-7 m/s and directions $270 - 280°$

Figure 5.6 displays the results for $280° - 290°$. The results for this directional band between the measured and the simulated results is closer than in figure 5.5. All the turbines are experiencing similar wake loss for both the measured and simulated values. Turbine four is showing the largest error between the measured and simulated values.

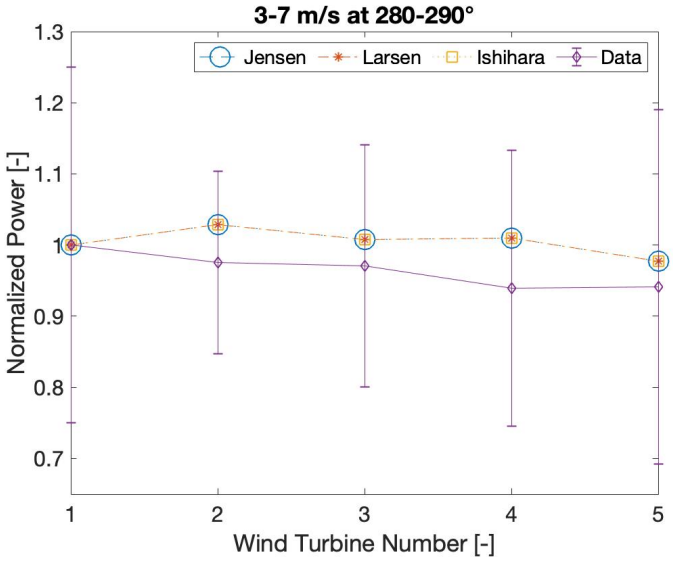

Figure 5.6: Simulated results compared with measured data for the velocity band 3-7 m/s and directions $280 - 290°$

Figure 5.7 displays the results for the directional band $290° - 300°$. The gap between the measured data and the simulated data has increased slightly from figure 5.6. All the wind

turbines are experiencing similar wake losses for the simulated results. Turbine two is showing the largest error between the measured and simulated data.

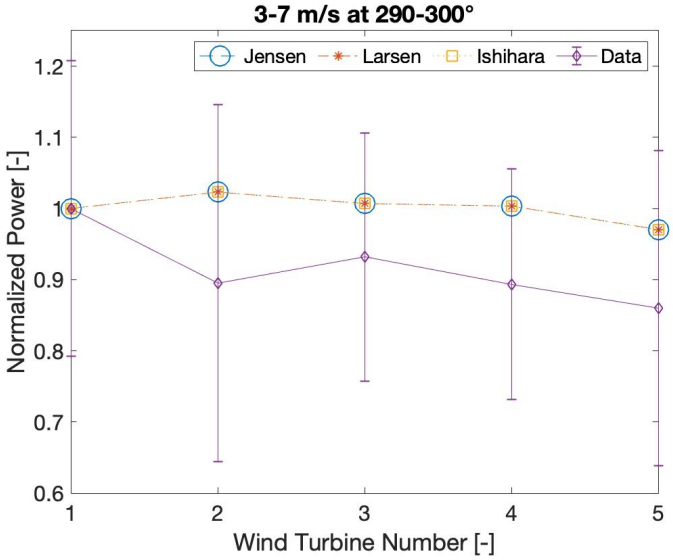

Figure 5.7: Simulated results compared with measured data for the velocity band 3-7 m/s and directions $290 - 300°$

Figure 5.8 displays the results for directional band $300° - 310°$. The difference between the measured and simulated results are smaller for this directional band than in figure 5.7. For wind turbines two and three the difference is not much, but the gap between the simulated and measured values is larger for turbines four and five.

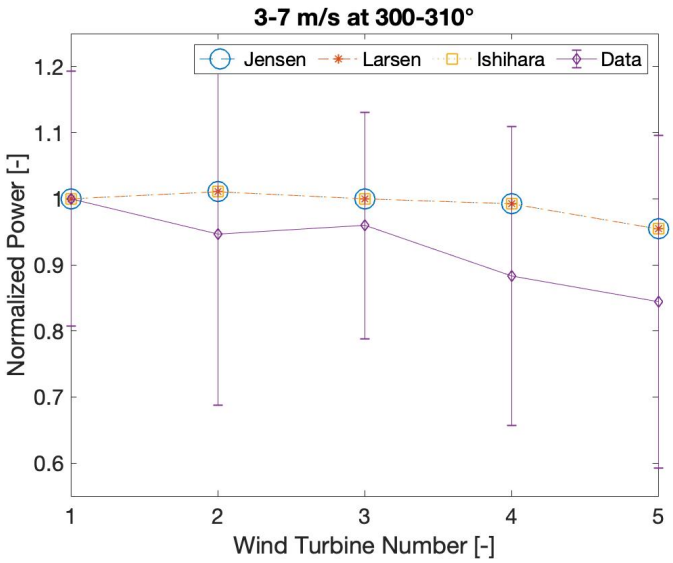

Figure 5.8: Simulated results compared with measured data for the velocity band 3-7 m/s and directions $300 - 310°$

Figure 5.9 displays the results for directional band $310° - 320°$. The simulated results show that wind turbines one, two, three, and four are all showing nearly the same wake loss for the simulated values, while turbine five is showing more wake loss. Turbine five is showing the smallest gap between the measured and simulated values, followed by turbine three then two. Turbine four is showing the largest error between the simulated and measured values.

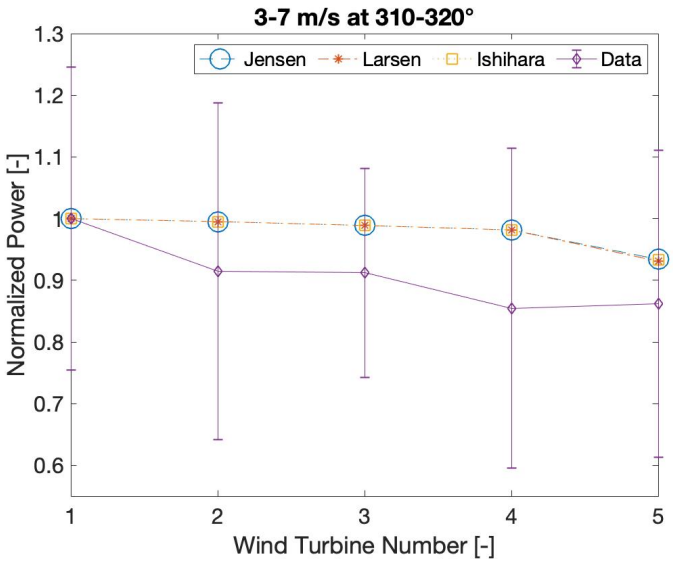

Figure 5.9: Simulated results compared with measured data for the velocity band 3-7 m/s and directions $310 - 320°$

5.2 Velocity band 7-11 m/s

In figure 5.19 the results for the directional band $230° - 240°$ are displayed. Turbine two is affected more wake than turbine one. The Ishihara wake model is showing the smallest wake loss, and is closest to the measured data, the Jensen model is showing slightly more wake loss than the Ishihara model, the Larsen wake model is showing the largest wake loss out of the models. Turbine three is showing the largest wake loss out of the wind turbines. The Larsen model is showing the smallest wake loss and is closest to the measured data. The Ishihara model is showing more wake loss than the Larsen model, and the Jensen model is showing the largest wake loss. Turbine four is experiencing the least amount of wake loss, as can be seen all the wake models are showing the same result. Turbine five shows the second largest amount of wake loss, and all the wake models are showing the same results for turbine five.

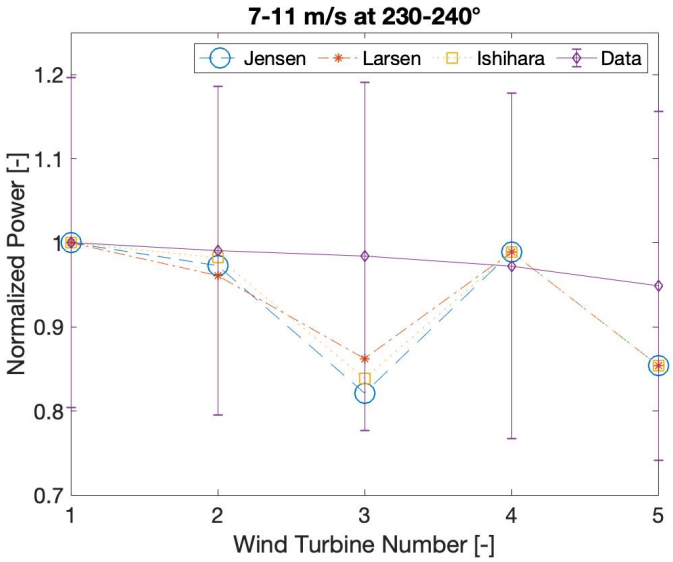

Figure 5.10: Simulated results compared with measured data for the velocity band 7-11 m/s and directions $230 - 240°$

Figure 5.11 displays the results for the directional band $240° - 250°$. Turbine two is affected by similar wake loss as turbine one. For turbine three the Larsen wake model is showing the most wake loss, and shows result closest to the measured data. The Ishihara and Jensen wake models are showing the same wake loss for turbine three. Turbine four is affected by the lowest wake of the turbines, and is also the turbine that has the largest gap between the measured and simulated data. Turbine five is being affected by the most wake loss out of the turbines. For turbines two, three, and five, the simulated data is very close to the measured data. Furthermore, for turbines two, four, and five all the wake models are showing the same wake loss for each wind turbine.

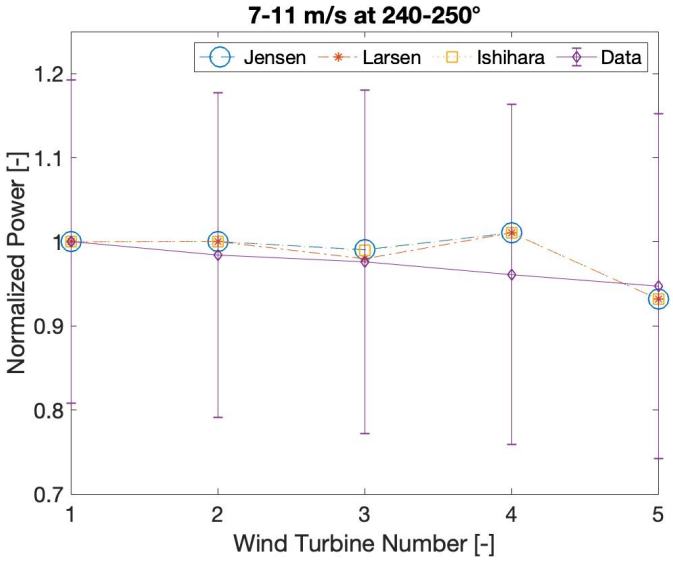

Figure 5.11: Simulated results compared with measured data for the velocity band 7-11 m/s and directions $240 - 250°$

Figure 5.12 displays the results for the directional band $250° - 260°$. As shown all the wake models are displaying the same results for each wind turbine. Wind turbines two, three and five are showing nearly the same wake loss and have values close to the measured data. The simulated values for turbine four show less wake loss. Turbine four also shows the largest gap between the measured and simulated value. This decrease in wake loss is not shown in the measured data but follows a similar value to the other turbines.

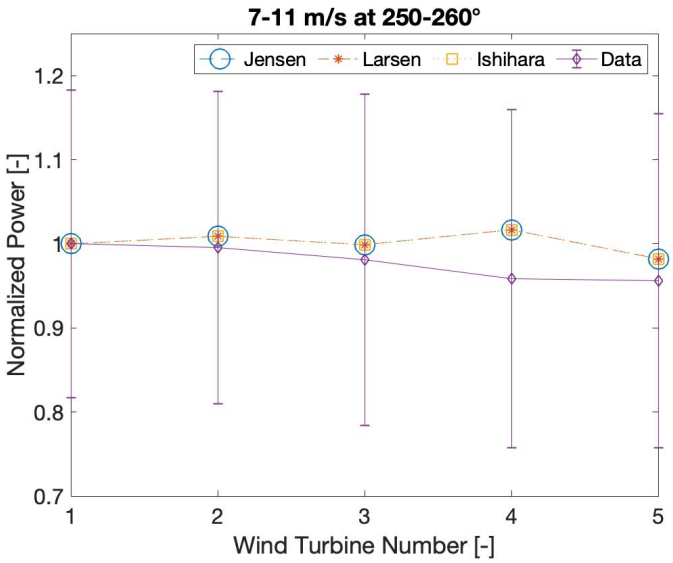

Figure 5.12: Simulated results compared with measured data for the velocity band 7-11 m/s and directions $250 - 260°$

Figure 5.13 displays the results for the directional band of $260° - 270°$. As for figure 5.12 the simulation results for turbine four are showing the least wake lake loss, and the largest gap between the simulation and measured data. For the other turbines they are all showing similar

wake loss to each other. All the wake models are showing the same wake loss for each wind turbine.

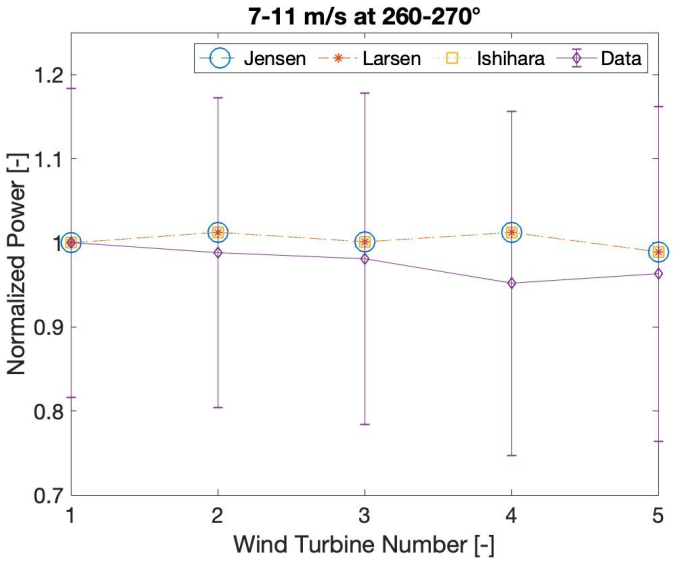

Figure 5.13: Simulated results compared with measured data for the velocity band 7-11 m/s and directions $260 - 270°$

Figure 5.14 displays the results from the directional band $270° - 280°$. All the turbines are are showing similar wake loss for the simulated values. The largest gap between the measured and simulated value is for turbine four, where the measured data shows a increase in wake loss compared to the other turbines. This is not represented in the simulated results. For wind turbine three the simulated and measured values are very close. The same goes for the results for turbine five. All the wake models are showing the same results for each wind turbine.

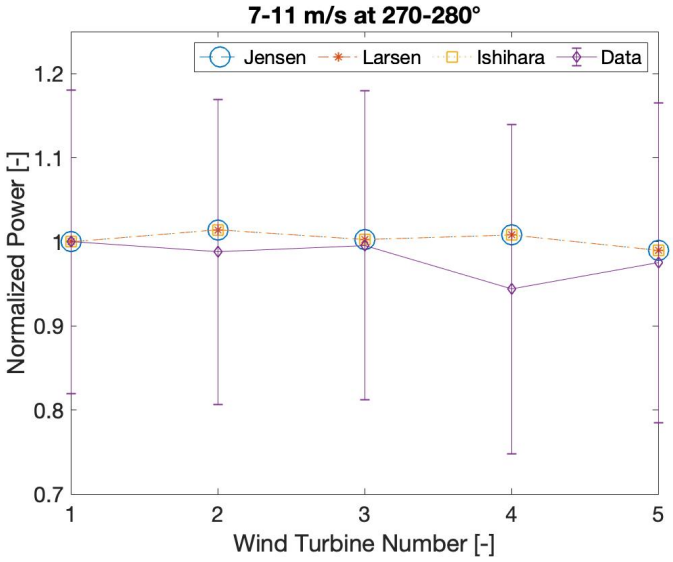

Figure 5.14: Simulated results compared with measured data for the velocity band 7-11 m/s and directions $270 - 280°$

Figure 5.15 displays the results for the directional band of $280° - 290°$. All the turbines are

showing similar wake loss to each other for the measured values. The largest gap between the measured and simulated data is for turbine four. The gap between the values is although smaller for this directional band than shown in figure 5.14. All the wake models are showing the same results for each wind turbine.

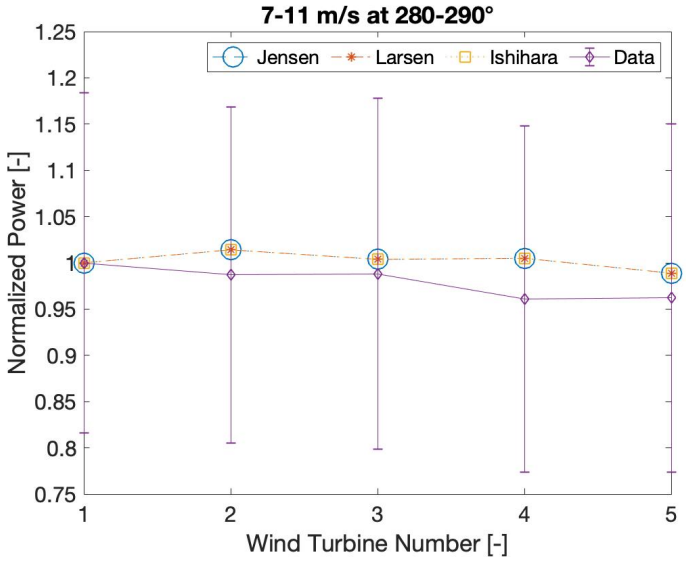

Figure 5.15: Simulated results compared with measured data for the velocity band 7-11 m/s and directions $280 - 290°$

Figure 5.16 displays the results for the directional band $290° - 300°$. All the wind turbines are showing similar wake losses and the difference from this directional band from figure 5.15 is minimal in the two graphs. All the wake models are showing the same results for each of the turbines.

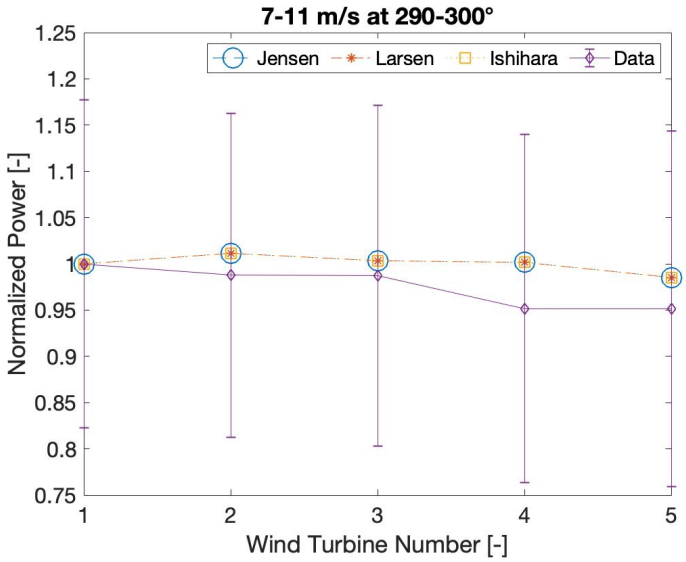

Figure 5.16: Simulated results compared with measured data for the velocity band 7-11 m/s and directions $290 - 300°$

Figure 5.17 displays the results for the directional band $290° - 300°$. All the wind turbines are

showing similar wake loss to each other for the simulated results. Wind turbine five though, shows the largest wake loss. The difference between the simulated value and the measured value is on the other hand non-distinguishable in the graph. The larger difference between the measured and simulated data is still for turbine four. The difference between the simulated and measured results for turbine three is also non-distinguishable on the graph same as for turbine five. All the wake models are showing the same results for each of the wind turbines.

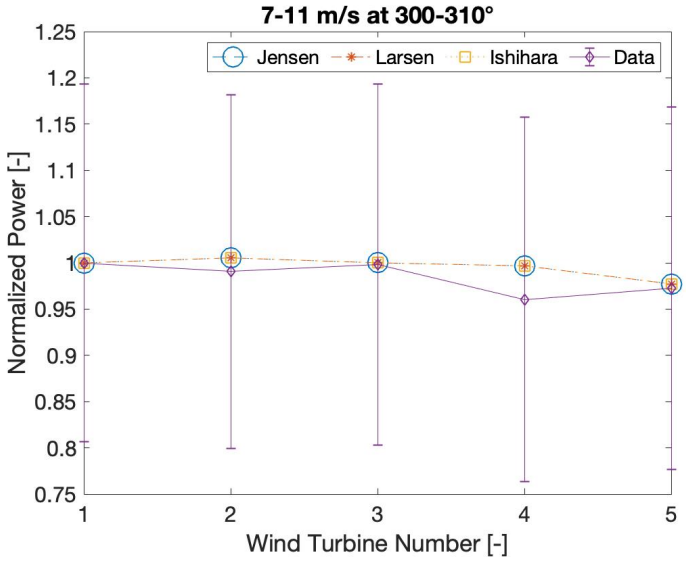

Figure 5.17: Simulated results compared with measured data for the velocity band 7-11 m/s and directions $300 - 310°$

Figure 5.18 displays the results for the directional band $310° - 320°$. All the simulated values for the wind turbines are show similar wake loss. With turbine five showing the largest wake loss, which has increased for this directional band compared to in figure 5.17. The gap between the measured and simulated results for turbine four has decreased from figure 5.17. Wind turbines two, three and five show such accurate simulation values that the difference from the measured values is non-distinguishable on the graph.

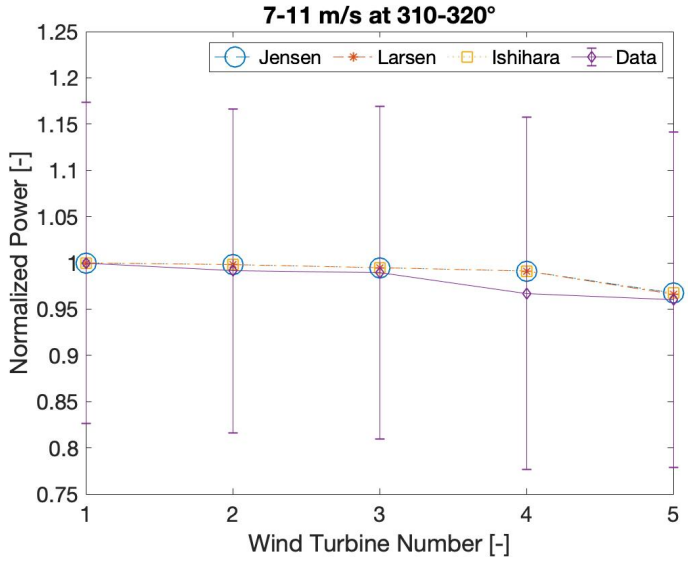

Figure 5.18: Simulated results compared with measured data for the velocity band 7-11 m/s and directions $310 - 320°$

5.3 Velocity band 11-15 m/s

Figure 5.19 displays the results for the directional band $230° - 240°$. As can be seen the simulated results for the wind turbines are showing similar wake loss. This is also the case for the measured data. For turbines two and five the measured and simulated data is nearly showing the same results. The error bar on the measured data are smaller compared to the 7-11 m/s velocity band, since the turbines' rated velocity is at 13 m/s, i.e. the rated power is achieved at this velocity band. Hence the power production is more stable. All the wake models are showing the same results for each wind turbine.

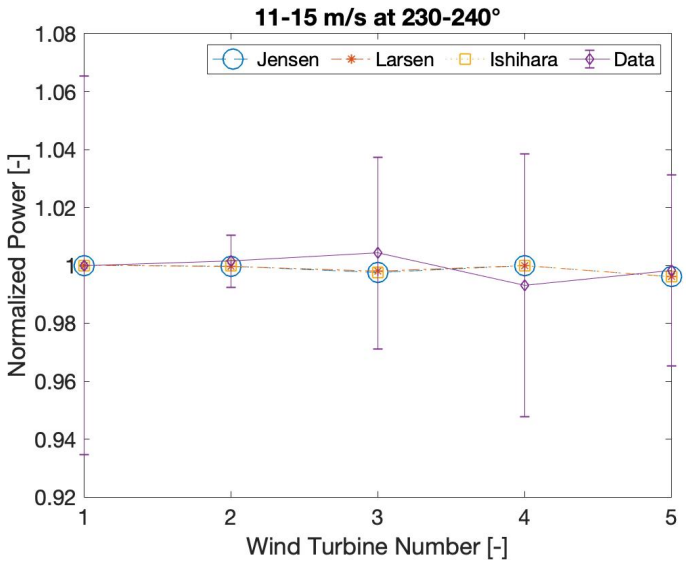

Figure 5.19: Simulated results compared with measured data for the velocity band 11-15 m/s and directions $230 - 240°$

Figure 5.20 displays the results for the directional band $240° - 250°$. All the wind turbines are showing similar wake loss. Wind turbine four is showing the most deviation compared to other turbines, with the simulated value showing smaller wake loss than the measured data. For turbine two, three, and five the measured and the simulated results show the same same results. All the wake models are showing the same solution for each wind turbine.

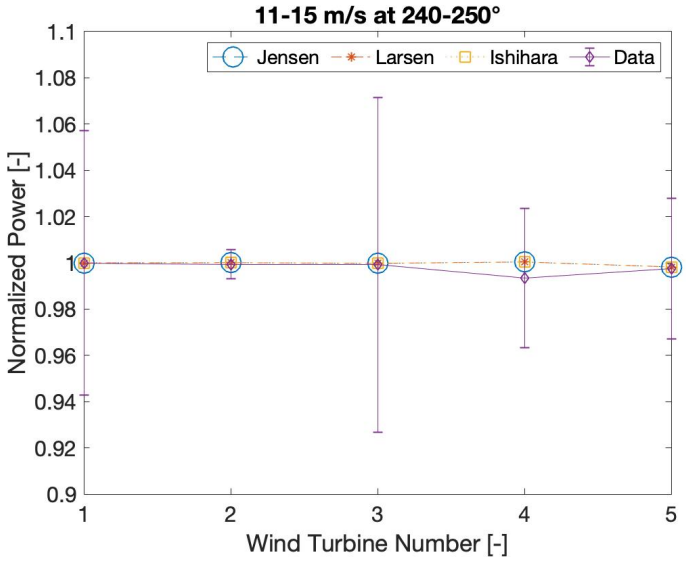

Figure 5.20: Simulated results compared with measured data for the velocity band 11-15 m/s and directions $240 - 250°$

Figure 5.21 displays the results for the directional band of $250° - 260°$. As shown the wind turbines are experiencing similar wake loss. Both for the measured and simulated results. Turbine four and five have the most deviation between the simulated and measured values. The deviation between the measured and simulated values for this directional band is smaller than in figure 5.20. Turbine three is showing high accuracy, compared to the measured data. All the wake models show the same solution for each wind turbine.

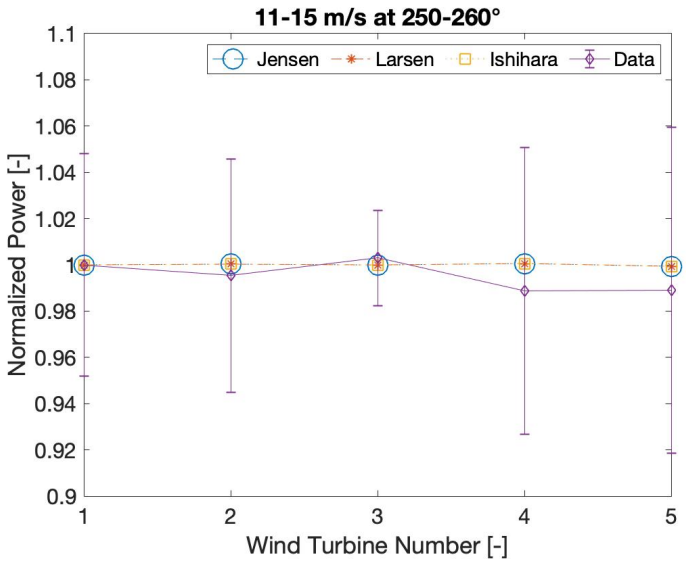

Figure 5.21: Simulated results compared with measured data for the velocity band 11-15 m/s and directions $250 - 260°$

Figure 5.22 display the result for the directional band of $260° - 270°$. All the wind turbines are experiencing similar wake loss in the simulated data. Turbine four has the largest error between the simulation and measured results. For turbine four the measured data has an increase in wake

loss, which is not represented in the simulation result. The error for turbine four has increased for this directional band from figure 5.21. The error for turbine five has decreased slightly for this directional band than in figure 5.21. While the results for turbines two and three have a similar result. All the wake models show the same solution for each wind turbine.

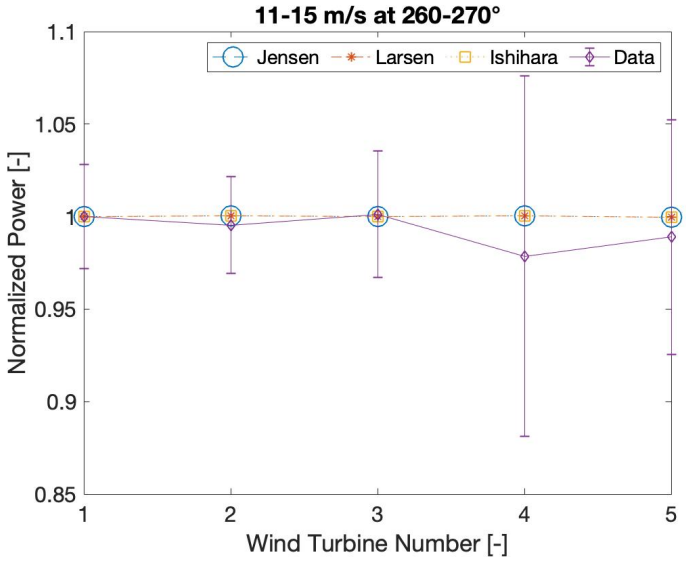

Figure 5.22: Simulated results compared with measured data for the velocity band 11-15 m/s and directions $260 - 270°$

Figure 5.23 displays the results for the directional band $270° - 280°$. The results for this directional band and in figure 5.22 show non-distinguishable differences in the graphs. All the wake models show the same solution for each wind turbine.

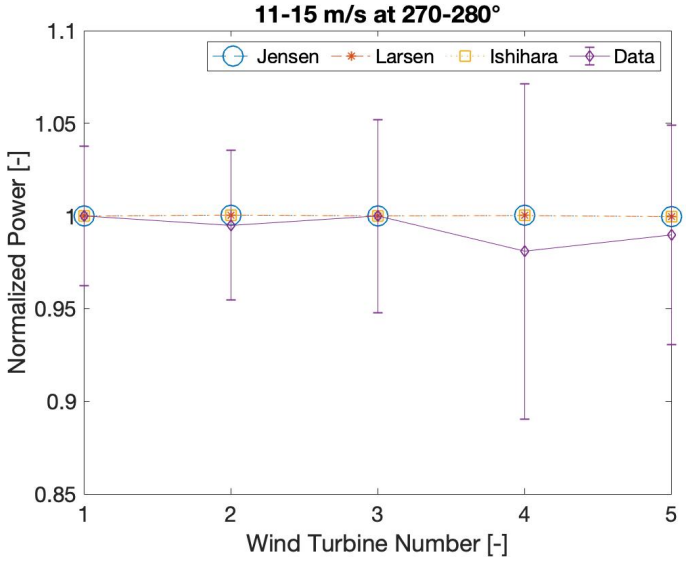

Figure 5.23: Simulated results compared with measured data for the velocity band 11-15 m/s and directions $270 - 280°$

Figure 5.24 displays the results from the directional band of $280° - 290°$. The results for this directional band are not showing much difference from figure 5.19. The main difference is the

result for turbine two. For this directional band the simulated value is closer to the measured result than in figure 5.23. All the wake models show the same solution for each wind turbine.

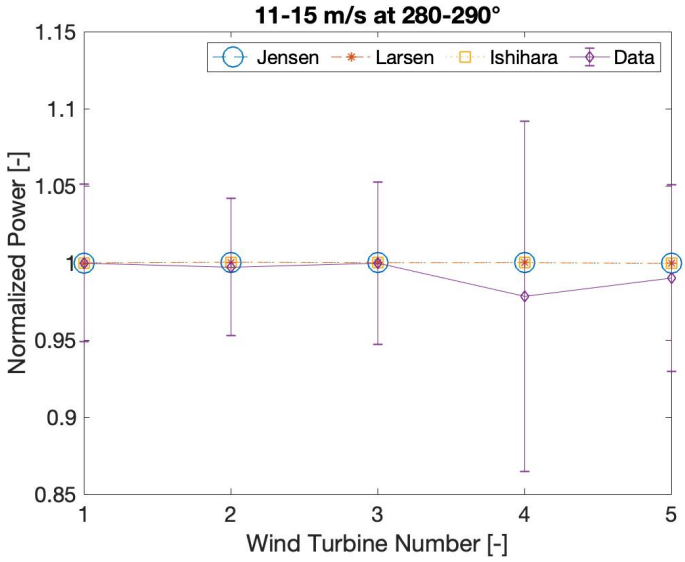

Figure 5.24: Simulated results compared with measured data for the velocity band 11-15 m/s and directions $280 - 290°$

Figure 5.25 displays the results for the directional band $290° - 300°$. As can be seen the results for this directional band don't show much difference from figure 5.24. The main difference is in the error bars on the measured data for turbines one, two, three and five. As can be seen the error bars are much smaller, and therefore the value of the measurements show more similar numbers. That means that the turbines are operating at rated power, or near the rated power at this velocity and directional band. But, this seem not to be the case for turbine four, which has a large error bar and therefor operating under different power at this velocity and directional band. All the wake models show the same solution for each wind turbine.

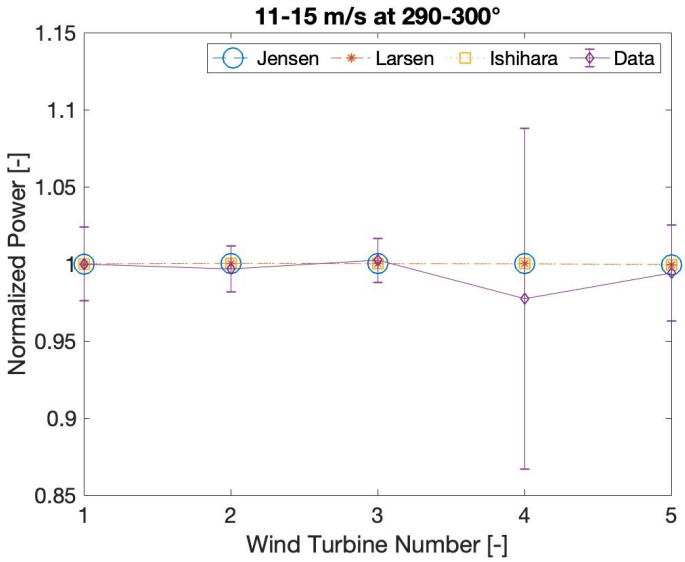

Figure 5.25: Simulated results compared with measured data for the velocity band 11-15 m/s and directions $290 - 300°$

Figure 5.26 displays the results for the directional band of $300° - 310°$. The results are similar to figure 5.25, but if looked at the error bars they have gotten larger for all the turbines. Meaning that the turbines are not operating as much at rated power as in figure 5.7. Turbine four still shows the largest error bar. All the wake models show the same solution for each wind turbine.

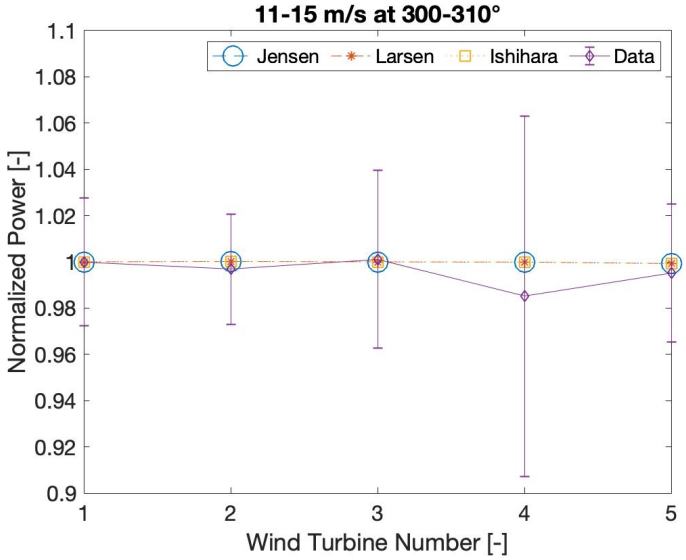

Figure 5.26: Simulated results compared with measured data for the velocity band 11-15 m/s and directions $300 - 310°$

Figure 5.27 displays the results for the directional band $310° - 320°$. As can be seen the results are similar to figure 5.26. The difference between the measured and simulated data for turbine four is smaller for this directional band, and for turbine five it is larger. It is interesting to see that this is the optimal velocity and directional band for turbine two, where it seems it is only operating at rated power. Turbine one stays the same as in figure 5.26. The error bars for turbines three, four and five have though increased.

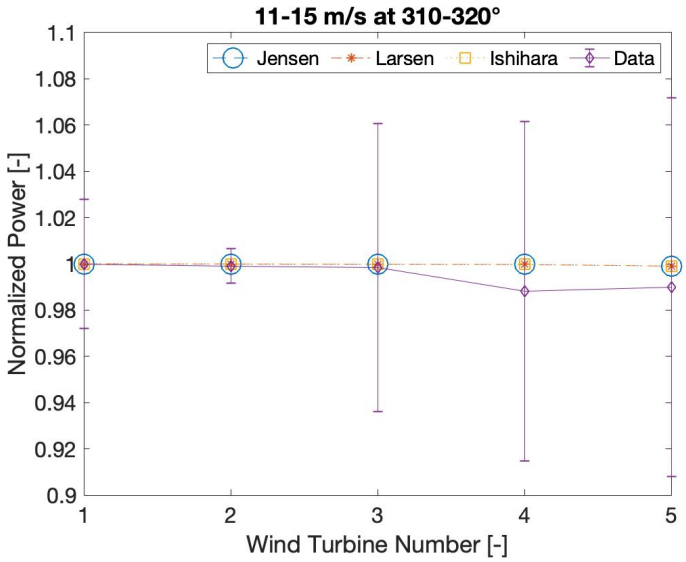

Figure 5.27: Simulated results compared with measured data for the velocity band 11-15 m/s and directions $310 - 320°$

5.4 Error Calculations

For the error calculations four different matrices were used. Root mean square error (RMSE), normalized root mean square error (NRMSE), and mean absolute error (MAE). The simulated results for all the wake models were compared with the measured values for all the velocity and directional bands analyzed in this project.

5.4.1 Root Mean Square Error

Figure 5.28 shows the RMSE results for the velocity band of 3-7 m/s. As can be seen all the wake models show similar results. The Larsen wake model has the smallest error. The Ishihara wake model gives the second best results. The Jensen model displays the most inaccuracy.

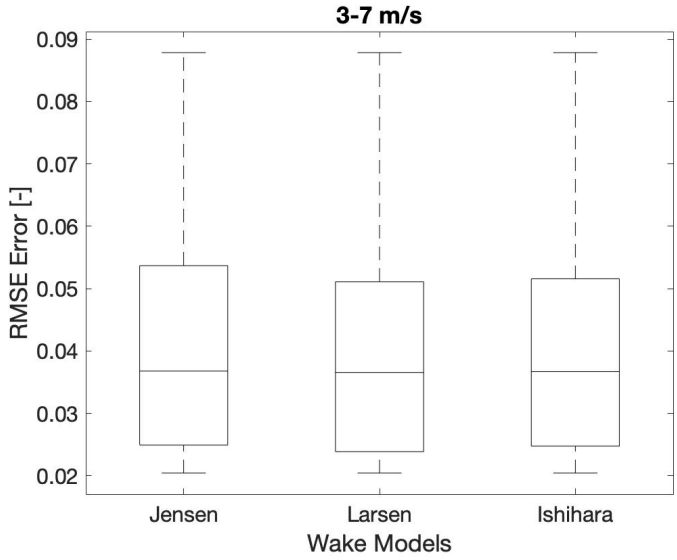

Figure 5.28: Root mean square error for the velocity band of 3-7 m/s.

The RMSE for the velocity band of 7-11 m/s is displayed in figure 5.29. The plus (+) signs in the figure represent the outliers of the measurements. The difference between the boxes of the error graph is non-distinguishable. As shown, the outliers give noticeable different results. With the Larsen model having the lowest error, Ishihara the second lowest and the Jensen showing the highest error of the outliers. This means that even though, the models give similar results for this velocity band, the Jensen model gives the highest out of place value. For all the wake models there is more accuracy at 7-11 m/s than at 3-7 m/s.

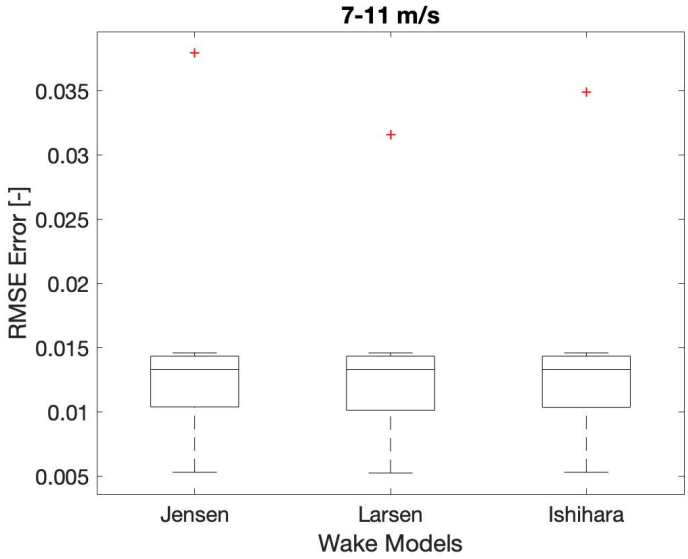

Figure 5.29: Root mean square error for the velocity band of 7-11 m/s.

Figure 5.30 shows the RMSE at the velocity band of 11-15 m/s. As shown, the difference between the errors of the wake models are non-distinguishable. According to the results shown in chapter 5.3, there is a slight difference between the wake models for the directional bands of $230° - 240°$ and $240° - 250°$. This difference is so small that it is non-distinguishable from the graphs. Hence the difference in error for this velocity band is negligible from the graph. Looking closer to the values obtained, the Larsen model does show the highest accuracy. The Jensen and Ishihara wake models are showing accuracy close to each other, with the Ishihara model slightly more accurate. For all the wake models the velocity band 11-15 m/s shows more accuracy than the other velocity bands. Please note that the y-axis in this graph is in 10^{-3}.

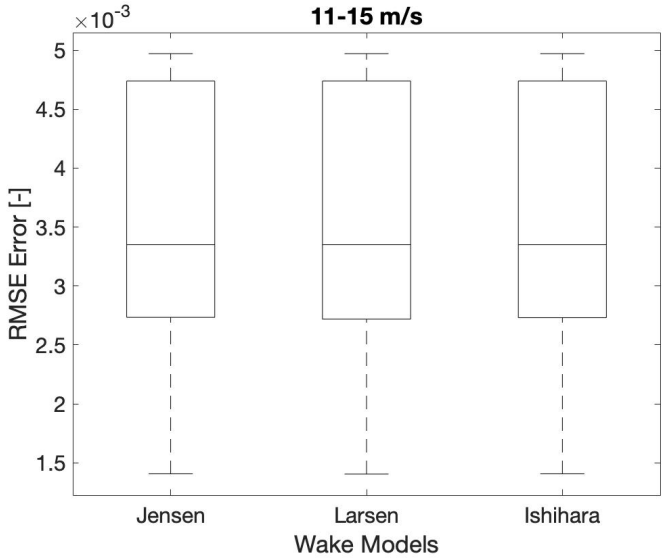

Figure 5.30: Root mean square error for the velocity band of 11-15 m/s.

5.4.2 Normalized Root Mean Square Error

Figure 5.31 shows the NRMSE for the velocity band of 3-7 m/s. The Larsen model is showing the highest accuracy. The Ishihara wake model is showing the second best accuracy, and the Jensen wake model is showing the most inaccuracy. Each wake model has one outlier that has the same value for all the wake models.

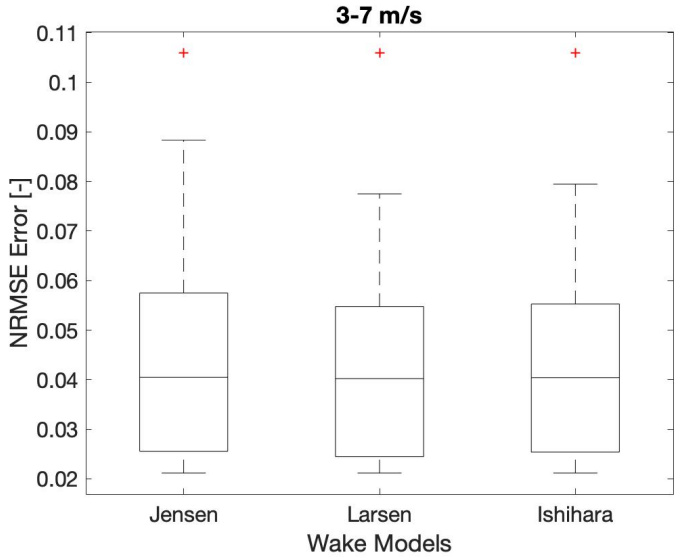

Figure 5.31: Normalized root mean squared error for the velocity band of 3-7 m/s.

Figure 5.32 shows the NRMSE for the velocity band of 7-11 m/s. The Jensen and Ishihara wake models show the slightly better results than the Larsen wake model in the box graph. As shown, the outliers show the Larsen wake model to have the smallest error, with Ishihara showing the second best results and the Jensen wake model showing the biggest error. As shown in the graph, differences between the models seem to be negligible, but looking at the outlier markers (+), the marker for the Larsen Wake model has the smallest error, and thus gave the best accuracy in the simulations. All the wake models are showing good accuracy. It is important to note that for all the wake models there is more accuracy at the velocity band of 7-11 m/s than at 3-7 m/s.

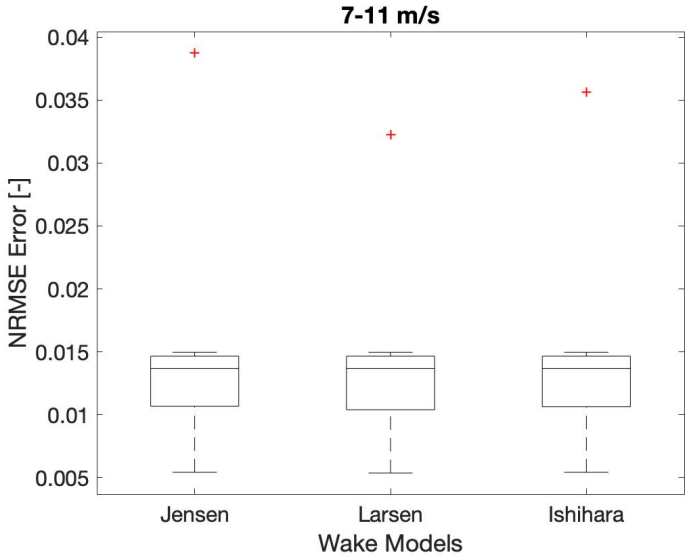

Figure 5.32: Normalized root mean squared error for the velocity band of 7-11 m/s.

Figure 5.33 displays the NRMSE for all three wake models for the velocity band of 11-15 m/s. As can be seen, the difference between the error of the wake models are non-distinguishable. This can be due to the fact in chapter 5.3, that there is a slight difference between the wake models for the directional bands of $230° - 240°$ and $240° - 250°$. This difference is, although so small that it is non-distinguishable from the graphs. Hence, the difference in error for this velocity band is not detectable in the graph. If taken a closer look at the results, the Larsen wake model is showing the most accuracy, while the Jensen and Ishihara wake models are showing similar results. The Ishihara wake model is, though showing slightly more accuracy. All the wake models are showing more accuracy for the velocity band of 11-15 m/s than for the 3-7 m/s and 7-11 m/s velocity bands respectively. Please note that the y-axis in this graph is in 10^{-3}.

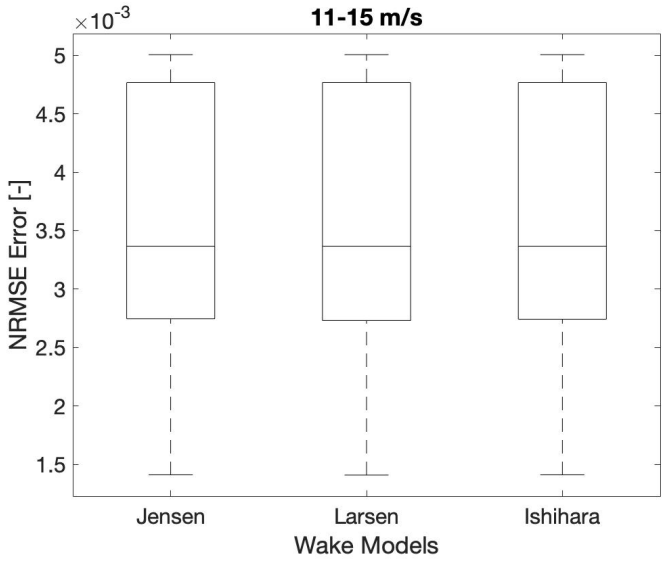

Figure 5.33: Normalized root mean squared error for the velocity band of 11-15 m/s.

5.4.3 Mean Absolute Error

Figure 5.34 shows the MAE results for the velocity band of 3-7 m/s. The Ishihara wake model is showing the most accuracy, though it is displaying an outlier that the other wake models are not showing. The Jensen and Larsen wake models are showing similar results. But the Larsen wake model shows slightly higher accuracy.

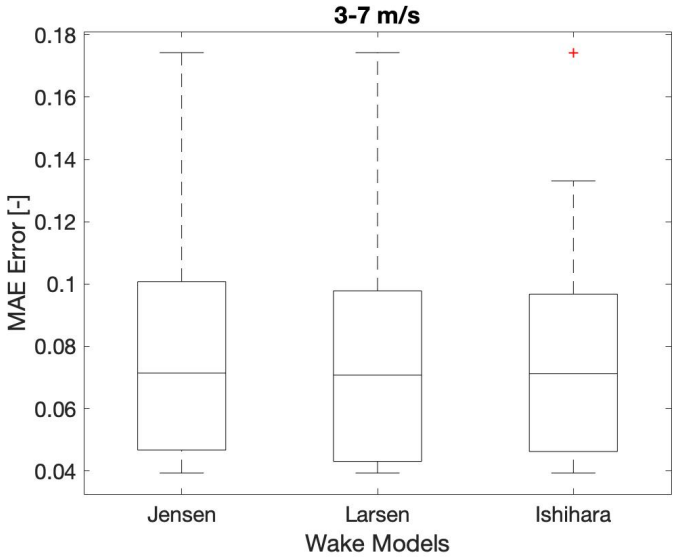

Figure 5.34: Mean absolute error for the velocity band of 3-7 m/s.

Figure 5.35 shows the MAE for the velocity band of 7-11 m/s. As can be seen, all the wake models are showing similar results. The Larsen model is showing the best accuracy, however, as shown the Larsen model shows higher amount of errors which are at lower values than the other wake models. All the wake models show the same high values. But, the outliers the Larsen model is also showing the lowest value. For the Jensen and Ishihara wake models the difference in the box graph is non-distinguishable. The Jensen model does have a higher value for the outlier than the Ishihara model, giving the Ishihara wake model a better overall result than the Jensen model. All the wake models are showing more accuracy for the velocity band of 7-11 m/s than for the velocity band of 3-7 m/s.

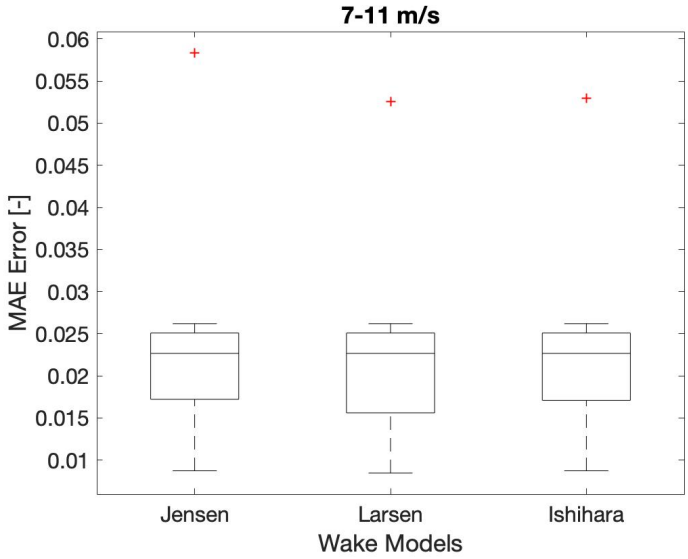

Figure 5.35: Mean absolute error for the velocity band of 7-11 m/s.

Figure 5.36 shows the MAE for the velocity band of 11-15 m/s. The difference between the errors of the wake models are negligible. As shown in chapter 5.3, there is a slight difference between the wake models for the directional bands of $230 - 240°$ and $240 - 250°$. On the other hand, this difference is so small that it is non-distinguishable in the graphs. Hence the difference in error for this velocity band is so small it's negligible. By looking closer into the results, it can be seen that the Larsen wake model has the smallest error. The Jensen and Ishihara wake models are showing similar result to each other, though the Ishihara wake model is showing a slightly smaller error. All the wake models are showing more accuracy for the velocity band of 11-15 m/s than for 3-7 m/s and 7-11 m/s. Please note that the y-axis in this graph is in 10^{-3}.

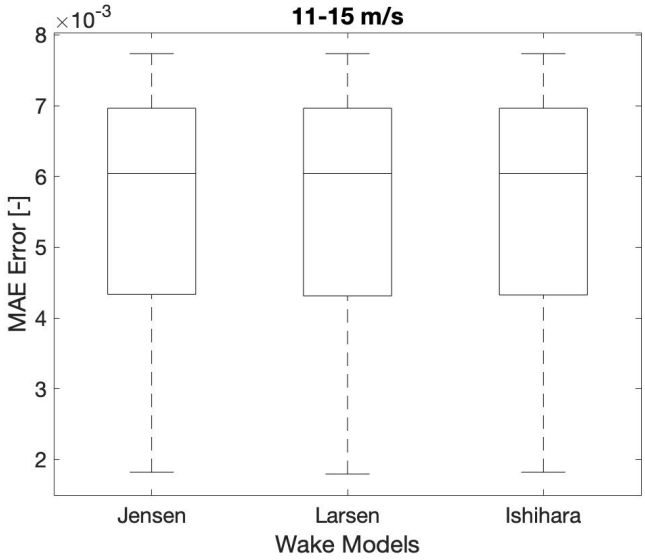

Figure 5.36: Mean absolute error for the velocity band of 11-15 m/s.

6 | Discussion

It was interesting to see how the Jensen, Larsen, and Ishihara wake models displayed the same wake loss for each wind turbine at all the directional bands, excluding the directional bands of $230° - 240°$ and $240° - 250°$. For the directional band $230 - 240°$ at the velocity bands 3-7 m/s and 7-11 m/s, it was seen that the wake models gave similar results for all the wind turbines except for turbine three, where the simulated data shows low wake loss for all the wake models. This decrease in wake loss is not represented by the measured data. For these specific parameters, the simulated results don't particularly follow the behavior of the measured data. But after these directional bands, the simulated results start to show closer similarities to the measured data. This can be due to the optimal angle of the wind turbines being west which is 270° and as the directional bands get closer to the optimal direction the more accurate the simulation becomes.

Out of the wind turbines, turbine four showed the biggest error between the measured and simulated results for all the velocity and directional bands. This could be due to the fact that for the measured values, turbine four seems to be affected by the wake from the other wind turbines, especially for the higher directional bands. This is understandable since turbine four is in line with turbines one, two, and three, and as the directional band increases the wind hits those turbines before turbine four, leaving it being affected by the wake of those turbines. It is also a possibility that turbine four needs maintenance for a technical problem since it is generating quite less overall power than the other turbines. This behaviour seems not to be represented in the simulation values, which show turbine four having similar wake loss to the other turbines or less wake loss than the other turbines. Leaving the error between the measured and simulated data larger. Turbine three also showed a high error from the measured and simulated results for the velocity bands of 3-7 m/s and 7-11 m/s, that could also be due to wake from other turbines since turbine three has other turbines close to it from both sides. Since for turbine three the measured value tends to show more wake loss than the simulated value, it could be a possibility that WindSim is not registering this effect from the other turbines. At the velocity band 11-15 m/s the results for turbine three are quite accurate, this can be due to the turbine stabilizing as it reaches the rated velocity of the turbine, which is 13 m/s. At 11-15 m/s the error between the measured and simulated values was small. Turbines two and five showed quite accurate results, though turbine two had a slightly better results than turbine five. Since turbine five for the velocity band 3-7 m/s, for the measured data turbine five is showing relatively low wake loss for directional bands $230 - 240°$ and $240 - 250°$. The simulated value is showing a large wake loss. The same goes for the directional band $230 - 240°$ at velocity band 7-11 m/s. Turbine five

should not have high wake loss since it is not in line with the other wind turbines, and hence should not be as effected by the wake of the other turbines. The accuracy for turbine one can't be disclaimed due to turbine one being the control turbine and having a value of one for all the wake models and measured data.

A factor that could be causing error between the measured data and the simulated data is that simulations don't take into account practical things that can happen. For example icing on the blades of the wind turbine. This is highly likely to happen to the turbines in the Wind R&D Park since it's located in Canada where the winters can be freezing. The icing can reduce the power production of the wind turbines. Also, torque affecting the turbines' rotor could cause some delay in power production when the turbine starts spinning or when the wind speed picks up or slows down.

For the over-all simulated results, turbine five is showing the lowest wake loss. But the second-lowest in the measured data. It makes sense that turbine five is showing low wake loss as it is further away from the other turbines and more inland, hence it is not in line with the other wind turbines and should not be as affected from the wake of the other turbines. The biggest difference from the simulated to the measured values is for turbine four, as mentioned before. Turbine four has the lowest wake loss for the measured results but the second-highest for the simulated results. The placement of the turbines is shown in table 6.1, where the turbine with the lowest wake loss is mention first, and the turbine with the highest wake loss is mentioned last. These placements don't change between velocity bands 3-7 m/s and 7-11 m/s. The results for the velocity band 11-15 m/s shows similar results between the simulated and measured values, Turbine four shows the lowest wake loss, and turbine five the second lowest. Other wind turbines were showing similar wake losses. The same applies to all the models. This can be due to the wind turbines rated velocity of the turbines is 13 m/s. This means that the turbines are operating at their most optimal and efficient velocity, hence producing rated power and therefore the wake loss across the wind farm is relatively even. This is also seen in the error calculations for RMSE, NRMSE and MAE as the velocity increases a smaller error between the measured and simulated values can be seen.

Table 6.1: Shows the total wake loss placement of the wind turbines. From lowest wake loss to highest.

Simulated result	**Measured result**
Turbine 5	Turbine 4
Turbine 3	Turbine 5
Turbine 1	Turbine 3
Turbine 4	Turbine 2
Turbine 2	Turbine 1

WindSim showed adequate results for wake effect simulations at the velocity and directional bands being studied. The results also showed a small error between the measured and simulated data. The program was easy to understand, user friendly, and fun to work with. The Wind R&D Park is though a small wind farm where the turbines are beside each other. Making the

behavior of the wake not as complex as for many other larger wind farms. Though WindSim performed well for the small wind farm being studied in this project, looking into larger wind farms with more complex wake behavior could give other results. As said before WindSim is easy to work with and gives adequate results, making it a good WFDT to get a basic picture of a wind farm's behavior or to get a rough estimate on capacity and turbine placement for new wind farms. Using another more complex program alongside WindSim is a great idea for the more in-depth and complex calculations, due to WindSim being a fairly simple program, especially for large wind farms with multiple turbines that affect each others wake losses.

7 | Conclusion

In this project, three wake models the Jensen, Larsen, and Ishihara were compared to each other. Results from simulations of each of the wake models were compared to the measured values of the Wind R&D Park in Canada, for the velocity bands of 3-7 m/s, 7-11 m/s and 11-15 m/s, and the directional band $230° - 320°$ where simulations were performed at $10°$ intervals. The aim of the project was to see how WindSim performs in wake modeling of a wind farm, how the simulated results compare to the measured values for every velocity and directional band.

For all the error calculations, which were RMSE, NRMSE, and MAE, the Larsen wake model showed the highest accuracy for all the velocity bands. The Ishihara wake model performed slightly better than the Jensen model. There was not much difference between the wake models for the directional band that was being studied, and as the velocity increased the more accurate the wake models became. This can be because as the velocity increases and gets closer to the turbines rated velocity, which is 13 m/s, the more stable the power production becomes. This makes the power generation of the wind turbines more predictable and the simulations more accurate, hence making the error between the measured and simulated values smaller. For some directional bands, all the wake models were showing similar wake loss. For all the velocity bands these directions were the same, or from $250° - 320°$. Leaving the only directional bands where the wake models show different results to $230° - 240°$ and $240° - 250°$ for all the velocity bands. The reason for this could be that as the directional band gets closer to $270°$ the more accurate the wake models become, since the most amount of the wind for the wind farm is coming from that direction, providing the most amount of data for the program, and hence the simulations show more accuracy and the wake models show the same or similar results. All the wake models were showing good results when compared to the measured data and are all adequate for predicting the wake loss for the wind farm.

WindSim performed adequately in simulating the wake losses of the Wind R&D Park. For all the velocity and directional bands, the simulated results were within the standard deviation of the measured values. Giving an acceptable error between the simulated and the measured values. The simulated values showed though results just below the standard deviation for the directional band $230 - 240°$ at the velocity 3-7 m/s. Turbine five showed just a slightly larger wake loss than the span of the standard deviation for that velocity and directional band. The Jensen model for turbine three also showed simulated values with higher wake loss than the standard deviation of the measured data for the earlier mentioned velocity and directional band.

8 | Further Research

In continuation of this project, conducting simulations for the rest of the directional band between $0 - 360°$ at $5°$ and testing out different turbulence models in combination with the wake models, would be interesting. To see if and how the turbulence model can change the outcome of the simulation. Turbulence models that would be interesting to look at could be standard k-epsilon, which is used in this project, Modified k-epsilon, and RNG k-epsilon. These turbulence models are also included in WindSim, which makes this step a natural step forward from this project. Other turbulence models that are included in WindSim and could be interesting to analyse combined with the wake are K-epsilon with YAP correction and K-omega model of Wilcox.

Furthermore, it could be interesting to test out other CFD programs, for example OpenWind or other similar programs and see if they give different results.

References

[1] N. Sedaghatizadeh, M. Arjomandi, R. Kelso, B. Cazzolato, and M. H. Ghayesh, "Modelling of wind turbine wake using large eddy simulation," *Renewable Energy*, vol. 115, pp. 1166–1176, 2018.

[2] F. Koch, M. Gresch, F. Shewarega, I. Erlich, and U. Bachmann, "Consideration of Wind Farm Wake Effect in Power System Dynamic Simulation," *IEEE Russia*, pp. 1–7, 2005.

[3] F. González-Longatt, P. P. Wall, and V. Terzija, "Wake effect in wind farm performance: Steady-state and dynamic behavior," *Renewable Energy*, vol. 39, no. 1, pp. 329–338, mar 2012.

[4] C. Kiranoudis and Z. Maroulis, "Effective Short-Cut Modelling of Wind Park Efficiency," *Renewable Energy*, vol. 11, pp. 439–457, 1997.

[5] P. B. Lissaman, "ENERGY EFFECTIVENESS OF ARBITRARY ARRAYS OF WIND TURBINES." *Journal of energy*, vol. 3, no. 6, pp. 323–328, may 1979.

[6] S. Voutsinas, K. Rados, and A. Zervos, "On the Analysis of Wake Effects in Wind Parks," Tech. Rep. 4, 1990.

[7] I. . Katic, J. . Højstrup, and N. O. Jensen, "A Simple Model for Cluster Efficiency," *European wind energy conference and exhibition*, vol. 1, pp. 407–410, 1986.

[8] WEICan, "About Us - Wind Energy Institute of Canada." [Online]. Available: https://www.weican.ca/about-us [Accessed: 2020-05-21]

[9] J.-O. Mo, A. Choudhry, M. Arjomandi, R. Kelso, and Y.-H. Lee, "Effects of wind speed changes on wake instability of a wind turbine in a virtual wind tunnel using large eddy simulation | Elsevier Enhanced Reader," *Journal of Wind Engineering and Industrial Aerodynamics*, vol. 117, pp. 38–56, 2013.

[10] M. De-Prada-Gil, C. G. Alías, O. Gomis-Bellmunt, and A. Sumper, "Maximum wind power plant generation by reducing the wake effect | Elsevier Enhanced Reader," *Energy Conversion and Management*, vol. 101, pp. 73–84, 2015.

[11] W. Zuo, X. Wang, and S. Kang, "Numerical simulations on the wake effect of H-type vertical axis wind turbines | Elsevier Enhanced Reader," *Energy*, vol. 106, pp. 691–700, 2016.

[12] Q. Li, T. Maeda, Y. Kamada, and Y. Hiromori, "Investigation of wake characteristic of a 30kW rated power Horizontal Axis Wind Turbine with wake model and field measurement | Elsevier Enhanced Reader," *Applied Energy*, vol. 225, pp. 1190–1204, 2018.

[13] A. Mittal, L. K. Taylor, K. Sreenivas, and A. Arabshahi, "Investigation of Two Analytical Wake Models Using Data From Wind Farms," in *Volume 6: Fluids and Thermal Systems; Advances for Process Industries, Parts A and B*. ASMEDC, jan 2011, pp. 1215–1222.

[14] N. Charhouni, A. Arbaoui, and M. Sallaou, "Qualification of three analytical wake models," Congrés Francais de Mécanique, Lyon, Tech. Rep., aug 2015.

[15] R. Shakoor, M. Y. Hassan, A. Raheem, and Y. K. Wu, "Wake effect modeling: A review of wind farm layout optimization using Jensen's model," *Renewable and Sustainable Energy Reviews*, vol. 58, pp. 1048–1059, may 2016.

[16] T. Göçmen, P. V. D. Laan, P. E. Réthoré, A. P. Diaz, G. C. Larsen, and S. Ott, "Wind turbine wake models developed at the technical university of Denmark: A review," *Renewable and Sustainable Energy Reviews*, vol. 60, pp. 752–769, jul 2016.

[17] H. Sun and H. Yang, "Study on three wake models' effect on wind energy estimation in Hong Kong," *Energy Procedia*, vol. 145, pp. 271–276, 2018.

[18] G. Crasto, A. Gravdahl, F. Castellani, and E. Piccioni, "Wake Modeling with the Actuator Disc Concept | Elsevier Enhanced Reader," *Energy Procedia*, vol. 24, pp. 385–392, jan 2012.

[19] F. Castellani, A. Gravdahl, G. Crasto, E. Piccioni, and A. Vignaroli, "A Practical Approach in the CFD Simulation of Off-shore Wind Farms through the Actuator Disc Technique | Elsevier Enhanced Reader," *Energy Procedia*, vol. 35, pp. 274–284, jan 2013.

[20] F. Castellani and A. Vignaroli, "An application of the actuator disc model for wind turbine wakes calculations | Elsevier Enhanced Reader," *Applied Energy*, vol. 101, pp. 432–440, jan 2013.

[21] N. Simisiroglou, S. P. Breton, G. Crasto, K. S. Hansen, and S. Ivanell, "Numerical CFD comparison of Lillgrund employing RANS," *Energy Procedia*, vol. 53, no. C, pp. 342–351, 2014.

[22] Y.-T. Wu and F. Porté-Agel, "Modeling turbine wakes and power losses within a wind farm using LES: An application to the Horns Rev offshore wind farm | Elsevier Enhanced Reader," *Renewable Energy*, vol. 75, pp. 945–955, mar 2015.

[23] F. Seim, A. R. Gravdahl, and M. S. Adaramola, "Validation of kinematic wind turbine wake models in complex terrain using actual windfarm production data | Elsevier Enhanced Reader," *Energy*, vol. 123, pp. 742–753, mar 2017.

[24] A. Crespo and J. Hernández, "Turbulence characteristics in wind-turbine wakes," *Journal of Wind Engineering and Industrial Aerodynamics*, vol. 61, no. 1, pp. 71–85, 1996.

[25] N. O. Jensen, "A note on wind generator interaction," Tech. Rep., 1983.

[26] J. G. Schepers, "ENDOW: Validation and improvement of ECN's wake model," Tech. Rep., mar 2003.

[27] I. Ammara, C. Leclerc, and C. Masson, "A viscous three-dimensional differential/actuator-disk method for the aerodynamic analysis of wind farms," *Journal of Solar Energy Engineering, Transactions of the ASME*, vol. 124, no. 4, pp. 345–356, nov 2002.

[28] T. Han, "The Assessmen of Dynamic Effects on Loading," Delft University of Technology, Delft, Tech. Rep., 2011.

[29] G. C. Larsen, "A simple stationary semi-analytical wake model," Tech. Rep., 2009.

[30] T. Ishihara, Y. Fujino, and A. Yamaguchi, "Development of a new wake model based on a wind tunnel experiment," The University of Tokyo, Tech. Rep., jan 2004.

[31] K. Azad and M. Saha, "(PDF) Weibull's Analysis of Wind Power Potential at Coastal Sites in Kuakata, Bangladesh," *International Journal of Energy Machinery*, vol. 4, pp. 36–45, aug 2011.

[32] W. A. S. Fjordgaten, "Getting Started," WindSim, Tønsberg, Tech. Rep., 2019.

[33] WindSim, "WindSim program," Tønsberg.

[34] V. Yakhot, T. Thangam, A. Orszag, and C. Speziale, "Development of Turbulence Models for Shear Flows by a Double Expansion technique." *Physics of Fluids A Fluid Dynamics*, aug 1992.

[35] N. Simisiroglou, "Wind power wake modelling Development and application of an actuator disc method for industrial utilization," Uppsala University, Uppsala, Tech. Rep., 2018.

[36] G. C. Larsen, "A Simple Wake Calculation Procedure," Technical University of Denmark, Tech. Rep., 1988.

[37] WEICan, "Facilities - Wind Energy Institute of Canada." [Online]. Available: https://www.weican.ca/facilities [Accessed: 2020-05-24]

[38] Global Mapper, "Global Mapper - All-in-one GIS Software," Maine. [Online]. Available: https://www.bluemarblegeo.com/products/global-mapper.php

[39] Windographer, "Windographer | Wind Resource Assessment Software," Albany. [Online]. Available: https://www.windographer.com/

Appendix A | Values used for the graphs

The values used to make all the graphs in the report are displayed for the simulations form WindSim

A.1 Simulations

3-7 m/s

Table A.1: Values for $230 - 240°$ at 3-7 m/s

Turbines	**Jensen**	**Larsen**	**Ishihara**	**Data**	**Standard deviation**
Turbine 1	1	1	1	1	0,224121
Turbine 2	0,921605	0,893802	0,949837	1,010626	0,116509
Turbine 3	0,594066	0,681949	0,646174	0,901514	0,263931
Turbine 4	0,969785	0,969785	0,969785	0,873792	0,252174
Turbine 5	0,706914	0,706914	0,706914	0,960293	0,241811

Table A.2: Values for $240 - 250°$ at 3-7 m/s

Turbines	**Jensen**	**Larsen**	**Ishihara**	**Data**	**Standard deviation**
Turbine 1	1	1	1	1	0,211729
Turbine 2	0,999807	0,999807	0,999807	1,035397	0,130993
Turbine 3	0,979627	0,95545	0,976641	0,930685	0,251593
Turbine 4	1,02124	1,02124	1,02124	0,962009	0,219776
Turbine 5	0,867216	0,867216	0,867216	0,963853	0,230549

Table A.3: Values for $250 - 260°$ at 3-7 m/s

Turbines	**Jensen**	**Larsen**	**Ishihara**	**Data**	**Standard deviation**
Turbine 1	1	1	1	1	0,1743
Turbine 2	1,018298	1,018298	1,018298	0,84165	0,265054
Turbine 3	0,997929	0,997929	0,997929	0,762471	0,252013
Turbine 4	1,034122	1,034122	1,034122	0,785375	0,266206
Turbine 5	0,964152	0,964152	0,964152	0,753513	0,26449

Table A.4: Values for $260 - 270°$ at 3-7 m/s

Turbines	**Jensen**	**Larsen**	**Ishihara**	**Data**	**Standard deviation**
Turbine 1	1	1	1	1	0,231421
Turbine 2	1,02558	1,02558	1,02558	0,967796	0,129314
Turbine 3	1,002315	1,002315	1,002315	0,888037	0,260386
Turbine 4	1,025699	1,025699	1,025699	0,869655	0,250406
Turbine 5	0,97804	0,97804	0,97804	0,895497	0,221797

Table A.5: Values for $270 - 280°$ at 3-7 m/s

Turbines	**Jensen**	**Larsen**	**Ishihara**	**Data**	**Standard deviation**
Turbine 1	1	1	1	1	0,205374
Turbine 2	1,029088	1,029088	1,029088	0,957433	0,158267
Turbine 3	1,005511	1,005511	1,005511	0,965652	0,149414
Turbine 4	1,016901	1,016901	1,016901	0,944744	0,209712
Turbine 5	0,979363	0,979363	0,979363	0,950679	0,235545

Table A.6: Values for $280 - 290°$ at 3-7 m/s

Turbines	**Jensen**	**Larsen**	**Ishihara**	**Data**	**Standard deviation**
Turbine 1	1	1	1	1	0,250116
Turbine 2	1,028735	1,028735	1,028735	0,9757	0,128401
Turbine 3	1,007714	1,007714	1,007714	0,970615	0,17018
Turbine 4	1,009951	1,009951	1,009951	0,939698	0,193774
Turbine 5	0,977271	0,977271	0,977271	0,941188	0,248793

Table A.7: Values for $290 - 300°$ at 3-7 m/s

Turbines	**Jensen**	**Larsen**	**Ishihara**	**Data**	**Standard deviation**
Turbine 1	1	1	1	1	0,207539
Turbine 2	1,023021	1,023021	1,023021	0,895123	0,250461
Turbine 3	1,006925	1,006925	1,006925	0,932032	0,174417
Turbine 4	1,003341	1,003341	1,003341	0,893438	0,162183
Turbine 5	0,970419	0,970419	0,970419	0,859833	0,221456

Table A.8: Values for $300 - 310°$ at 3-7 m/s

Turbines	**Jensen**	**Larsen**	**Ishihara**	**Data**	**Standard deviation**
Turbine 1	1	1	1	1	0,193016
Turbine 2	1,01061	1,01061	1,01061	0,946699	0,258563
Turbine 3	0,999942	0,999942	0,999942	0,959553	0,171114
Turbine 4	0,992426	0,992426	0,992426	0,883244	0,22608
Turbine 5	0,954331	0,954331	0,954331	0,844375	0,251868

Table A.9: Values for $310 - 320°$ at 3-7 m/s

Turbines	**Jensen**	**Larsen**	**Ishihara**	**Data**	**Standard deviation**
Turbine 1	1	1	1	1	0,245695
Turbine 2	0,995145	0,995145	0,995145	0,91437	0,273189
Turbine 3	0,988852	0,988852	0,988852	0,911909	0,169828
Turbine 4	0,981659	0,981659	0,981659	0,854544	0,259331
Turbine 5	0,934069	0,930832	0,933229	0,861823	0,249253

7-11 m/s

Table A.10: Values for $230 - 240°$ at 7-11 m/s

Turbines	**Jensen**	**Larsen**	**Ishihara**	**Data**	**Standard deviation**
Turbine 1	1	1	1	1	0,196197586
Turbine 2	0,972878005	0,961015502	0,98227814	0,990718679	0,195041856
Turbine 3	0,821316558	0,86235902	0,838822736	0,983958564	0,207225002
Turbine 4	0,989036172	0,989036172	0,989036172	0,972452589	0,205209416
Turbine 5	0,854127162	0,854127162	0,854127162	0,948956766	0,207254535

Table A.11: Values for $240 - 250°$ at 7-11 m/s

Turbines	**Jensen**	**Larsen**	**Ishihara**	**Data**	**Standard deviation**
Turbine 1	1	1	1	1	0,192231229
Turbine 2	1,000370193	1,000370193	1,000370193	0,984429875	0,193138517
Turbine 3	0,99061512	0,979869532	0,989744667	0,975994611	0,204053066
Turbine 4	1,010675551	1,010675551	1,010675551	0,961079599	0,202115849
Turbine 5	0,931824549	0,931824549	0,931824549	0,947218864	0,205318311

Table A.12: Values for $250 - 260°$ at 7-11 m/s

Turbines	**Jensen**	**Larsen**	**Ishihara**	**Data**	**Standard deviation**
Turbine 1	1	1	1	1	0,183073026
Turbine 2	1,008884168	1,008884168	1,008884168	0,995225184	0,185791226
Turbine 3	0,998918449	0,998918449	0,998918449	0,981218592	0,196862207
Turbine 4	1,016773695	1,016773695	1,016773695	0,958576287	0,201188925
Turbine 5	0,982183381	0,982183381	0,982183381	0,956296586	0,198455172

Table A.13: Values for $260 - 270°$ at 7-11 m/s

Turbines	**Jensen**	**Larsen**	**Ishihara**	**Data**	**Standard deviation**
Turbine 1	1	1	1	1	0,183470949
Turbine 2	1,012556509	1,012556509	1,012556509	0,988336812	0,18426153
Turbine 3	1,001200972	1,001200972	1,001200972	0,981218266	0,196990343
Turbine 4	1,012322173	1,012322173	1,012322173	0,951761694	0,204390766
Turbine 5	0,989327944	0,989327944	0,989327944	0,963090585	0,198886607

Table A.14: Values for $270 - 280°$ at 7-11 m/s

Turbines	**Jensen**	**Larsen**	**Ishihara**	**Data**	**Standard deviation**
Turbine 1	1	1	1	1	0,180403349
Turbine 2	1,014272299	1,014272299	1,014272299	0,987900185	0,181251925
Turbine 3	1,002724289	1,002724289	1,002724289	0,995842923	0,183630394
Turbine 4	1,008154271	1,008154271	1,008154271	0,943835511	0,19578572
Turbine 5	0,989874571	0,989874571	0,989874571	0,97527444	0,190173015

Table A.15: Values for $280 - 290°$ at 7-11 m/s

Turbines	**Jensen**	**Larsen**	**Ishihara**	**Data**	**Standard deviation**
Turbine 1	1	1	1	1	0,183957388
Turbine 2	1,014103816	1,014103816	1,014103816	0,986972568	0,181691833
Turbine 3	1,00375601	1,00375601	1,00375601	0,988183692	0,189645499
Turbine 4	1,004920373	1,004920373	1,004920373	0,960953095	0,187304788
Turbine 5	0,988872822	0,988872822	0,988872822	0,962195664	0,188270117

Table A.16: Values for $290 - 300°$ at 7-11 m/s

Turbines	**Jensen**	**Larsen**	**Ishihara**	**Data**	**Standard deviation**
Turbine 1	1	1	1	1	0,177131988
Turbine 2	1,011402019	1,011402019	1,011402019	0,98787441	0,175120899
Turbine 3	1,003416701	1,003416701	1,003416701	0,986946339	0,184171425
Turbine 4	1,001620492	1,001620492	1,001620492	0,951754019	0,188491822
Turbine 5	0,985239852	0,985239852	0,985239852	0,951552977	0,192212435

Table A.17: Values for $300 - 310°$ at 7-11 m/s

Turbines	**Jensen**	**Larsen**	**Ishihara**	**Data**	**Standard deviation**
Turbine 1	1	1	1	1	0,193054469
Turbine 2	1,005363208	1,005363208	1,005363208	0,9906734	0,1911062
Turbine 3	1,000019864	1,000019864	1,000019864	0,998205565	0,195064388
Turbine 4	0,996772143	0,996772143	0,996772143	0,960435006	0,196946299
Turbine 5	0,977265956	0,977265956	0,977265956	0,972455144	0,196063281

Table A.18: Values for $310 - 320°$ at 7-11 m/s

Turbines	**Jensen**	**Larsen**	**Ishihara**	**Data**	**Standard deviation**
Turbine 1	1	1	1	1	0,173311252
Turbine 2	0,998121998	0,998121998	0,998121998	0,991260523	0,175258319
Turbine 3	0,994801772	0,994801772	0,994801772	0,989399107	0,179887784
Turbine 4	0,991149524	0,991149524	0,991149524	0,967007459	0,190198756
Turbine 5	0,967409913	0,966050696	0,967409913	0,96018151	0,181138028

11-15 m/s

Table A.19: Values for $230 - 240°$ at 11-15 m/s

Turbines	Jensen	Larsen	Ishihara	Data	Standard deviation
Turbine 1	1	1	1	1	0,065459832
Turbine 2	0,999696135	0,99961231	0,99977996	1,001433227	0,008985746
Turbine 3	0,997516686	0,99799868	0,997590033	1,004213995	0,033169877
Turbine 4	0,999905697	0,999905697	0,999905697	0,993153331	0,045399135
Turbine 5	0,99604975	0,99604975	0,99604975	0,998245797	0,033014839

Table A.20: Values for $240 - 250°$ at 11-15 m/s

Turbines	Jensen	Larsen	Ishihara	Data	Standard deviation
Turbine 1	1	1	1	1	0,057070288
Turbine 2	1,000062317	1,000062317	1,000062317	0,999372814	0,006381101
Turbine 3	0,999795243	0,999795243	0,999795243	0,999126844	0,072368922
Turbine 4	1,000365002	1,000365002	1,000365002	0,99344292	0,030035578
Turbine 5	0,998228403	0,998228403	0,998228403	0,997399875	0,030417138

Table A.21: Values for $250 - 260°$ at 11-15 m/s

Turbines	Jensen	Larsen	Ishihara	Data	Standard deviation
Turbine 1	1	1	1	1	0,04803939
Turbine 2	1,000299763	1,000299763	1,000299763	0,995357373	0,050407666
Turbine 3	0,99996253	0,99996253	0,99996253	1,003052188	0,020596593
Turbine 4	1,000571423	1,000571423	1,000571423	0,988773354	0,062028309
Turbine 5	0,999391106	0,999391106	0,999391106	0,98902016	0,070412157

Table A.22: Values for $260 - 270°$ at 11-15 m/s

Turbines	Jensen	Larsen	Ishihara	Data	Standard deviation
Turbine 1	1	1	1	1	0,028087897
Turbine 2	1,000413903	1,000413903	1,000413903	0,995459845	0,026280443
Turbine 3	1,000036791	1,000036791	1,000036791	1,001207268	0,034174511
Turbine 4	1,000413903	1,000413903	1,000413903	0,978567641	0,097419992
Turbine 5	0,999641284	0,999641284	0,999641284	0,988938019	0,06349607

Table A.23: Values for $270 - 280°$ at 11-15 m/s

Turbines	**Jensen**	**Larsen**	**Ishihara**	**Data**	**Standard deviation**
Turbine 1	1	1	1	1	0.037746868
Turbine 2	1,000485305	1,000485305	1,000485305	0,994942193	0.040373311
Turbine 3	1,000097061	1,000097061	1,000097061	0,999857178	0.052222624
Turbine 4	1,000262065	1,000262065	1,000262065	0,980898321	0.090503526
Turbine 5	0,99965058	0,99965058	0,99965058	0,989840608	0.059321805

Table A.24: Values for $280 - 290°$ at 11-15 m/s

Turbines	**Jensen**	**Larsen**	**Ishihara**	**Data**	**Standard deviation**
Turbine 1	1	1	1	1	0,051187824
Turbine 2	1,000420554	1,000420554	1,000420554	0,997366855	0,044370955
Turbine 3	1,000109033	1,000109033	1,000109033	0,999834774	0,052695304
Turbine 4	1,000147973	1,000147973	1,000147973	0,978290591	0,113572928
Turbine 5	0,999665114	0,999665114	0,999665114	0,99008233	0,060560906

Table A.25: Values for $290 - 300°$ at 11-15 m/s

Turbines	**Jensen**	**Larsen**	**Ishihara**	**Data**	**Standard deviation**
Turbine 1	1	1	1	1	0,023811374
Turbine 2	1,000370514	1,000370514	1,000370514	0,996771666	0,01506447
Turbine 3	1,000114683	1,000114683	1,000114683	1,002305846	0,014201052
Turbine 4	1,000052931	1,000052931	1,000052931	0,977505314	0,110437942
Turbine 5	0,999514803	0,999514803	0,999514803	0,994105652	0,031250369

Table A.26: Values for $300 - 310°$ at 11-15 m/s

Turbines	**Jensen**	**Larsen**	**Ishihara**	**Data**	**Standard deviation**
Turbine 1	1	1	1	1	0,027580254
Turbine 2	1,000170949	1,000170949	1,000170949	0,996791671	0,023731573
Turbine 3	1	1	1	1,001148586	0,038372352
Turbine 4	0,999897431	0,999897431	0,999897431	0,985160459	0,077958011
Turbine 5	0,999273467	0,999273467	0,999273467	0,995204219	0,029853664

Table A.27: Values for $310 - 320°$ at 11-15 m/s

Turbines	**Jensen**	**Larsen**	**Ishihara**	**Data**	**Standard deviation**
Turbine 1	1	1	1	1	0,027872356
Turbine 2	1,000170949	0,999943013	0,999943013	0,999030842	0,007477615
Turbine 3	0,999943013	0,999845321	0,999845321	0,998504964	0,062300174
Turbine 4	0,999731347	0,999731347	0,999731347	0,988088646	0,073338799
Turbine 5	0,999006798	0,999006798	0,999006798	0,989810957	0,08183711

A.2 Error Calculations

RMSE

Table A.28: Values for RMSE at 3-7 m/s

Direction [°]	**Jensen**	**Larsen**	**Ishihara**
230-240	0,08387238	0,073558736	0,075447871
240-250	0,02569759	0,024271036	0,025476088
250-260	0,087838214	0,087838214	0,087838214
260-270	0,043617232	0,043617232	0,043617232
270-280	0,022585519	0,022585519	0,022585519
280-290	0,020422048	0,020422048	0,020422048
290-300	0,04302309	0,04302309	0,04302309
300-310	0,034610077	0,034610077	0,034610077
310-320	0,036781678	0,036532235	0,036716075

Table A.29: Values for RMSE at 7-11 m/s

Direction [°]	**Jensen**	**Larsen**	**Ishihara**
230-240	0,037967555	0,031582525	0,034873096
240-250	0,011250949	0,010891928	0,011206964
250-260	0,013500988	0,013500988	0,013500988
260-270	0,014617624	0,014617624	0,014617624
270-280	0,014272923	0,014272923	0,014272923
280-290	0,012038927	0,012038927	0,012038927
290-300	0,013336104	0,013336104	0,013336104
300-310	0,007905982	0,007905982	0,007905982
310-320	0,005334258	0,005267088	0,005334258

Table A.30: Values for RMSE at 11-15 m/s

Direction [°]	Jensen	Larsen	Ishihara
230-240	0,001982811	0,001922113	0,001970048
240-250	0,001407464	0,001405179	0,001407464
250-260	0,003350965	0,003350965	0,003350965
260-270	0,004970842	0,004970842	0,004970842
270-280	0,004480954	0,004480954	0,004480954
280-290	0,004812381	0,004812381	0,004812381
290-300	0,004713414	0,004713414	0,004713414
300-310	0,00313991	0,00313991	0,00313991
310-320	0,002984926	0,002984926	0,002984926

NRMSE

Table A.31: Values for NRMSE at 3-7 m/s

Direction [°]	Jensen	Larsen	Ishihara
230-240	0,088356953	0,077491849	0,079481994
240-250	0,026265215	0,02480715	0,02603882
250-260	0,10600777	0,10600777	0,10600777
260-270	0,047194738	0,047194738	0,047194738
270-280	0,023436218	0,023436218	0,023436218
280-290	0,021153096	0,021153096	0,021153096
290-300	0,046964071	0,046964071	0,046964071
300-310	0,037344676	0,037344676	0,037344676
310-320	0,040484855	0,040210298	0,040412647

Table A.32: Values for NRMSE at 7-11 m/s

Direction [°]	Jensen	Larsen	Ishihara
230-240	0,038773369	0,032252825	0,035613234
240-250	0,011554312	0,01118561	0,011509141
250-260	0,013800976	0,013800976	0,013800976
260-270	0,014963559	0,014963559	0,014963559
270-280	0,014555732	0,014555732	0,014555732
280-290	0,01228887	0,01228887	0,01228887
290-300	0,013669286	0,013669286	0,013669286
300-310	0,008031646	0,008031646	0,008031646
310-320	0,005434416	0,005365984	0,005434416

Table A.33: Values for NRMSE at 11-15 m/s

Direction [°]	**Jensen**	**Larsen**	**Ishihara**
230-240	0,001983983	0,001923249	0,001971212
240-250	0,00141047	0,00140818	0,00141047
250-260	0,00336699	0,00336699	0,00336699
260-270	0,005006718	0,005006718	0,005006718
270-280	0,004512053	0,004512053	0,004512053
280-290	0,004845744	0,004845744	0,004845744
290-300	0,004741209	0,004741209	0,004741209
300-310	0,003153594	0,003153594	0,003153594
310-320	0,002999663	0,002999663	0,002999663

MAE

Table A.34: Values for MAE at 3-7 m/s

Direction [°]	**Jensen**	**Larsen**	**Ishihara**
230-240	0,149168111	0,137152246	0,133100294
240-250	0,048080237	0,043244712	0,04748302
250-260	0,174298394	0,174298394	0,174298394
260-270	0,082129859	0,082129859	0,082129859
270-280	0,042471165	0,042471165	0,042471165
280-290	0,039293982	0,039293982	0,039293982
290-300	0,084655855	0,084655855	0,084655855
300-310	0,064887786	0,064887786	0,064887786
310-320	0,071415526	0,070768199	0,0712477

Table A.35: Values for MAE at 7-11 m/s

Direction [°]	**Jensen**	**Larsen**	**Ishihara**
230-240	0,058379173	0,052543181	0,05299791
240-250	0,019110219	0,016961101	0,018936128
250-260	0,023088609	0,023088609	0,023088609
260-270	0,026200048	0,026200048	0,026200048
270-280	0,022434474	0,022434474	0,022434474
280-290	0,0226696	0,0226696	0,0226696
290-300	0,024710264	0,024710264	0,024710264
300-310	0,011530411	0,011530411	0,011530411
310-320	0,008726922	0,008455078	0,008726922

Table A.36: Values for MAE at 11-15 m/s

Direction [°]	**Jensen**	**Larsen**	**Ishihara**
230-240	0,003476563	0,003396929	0,003445128
240-250	0,001821702	0,001794995	0,001821702
250-260	0,006040213	0,006040213	0,006040213
260-270	0,007734813	0,007734813	0,007734813
270-280	0,006991342	0,006991342	0,006991342
280-290	0,006953625	0,006953625	0,006953625
290-300	0,006749356	0,006749356	0,006749356
300-310	0,004666817	0,004666817	0,004666817
310-320	0,004618214	0,004618214	0,004618214